Hyaluronic acid hydrogels reinforced with laser spun bioactive glass micro- and nanofibres doped with lithium

Antonio Riveiro, Sara Amorim, Anu Solanki, Diana S. Costa, Ricardo A. Pires, Félix Quintero, Jesús del Val, Rafael Comesaña, Aida Badaoui, Fernando Lusquiños, Anthony L.B. Maçon, Francesca Tallia, Julian R. Jones, Rui L. Reis, Juan Pou.*

Dr. A. Riveiro[1*], Dr. F. Quintero[2], Dr. J. del Val[2], Dr. R. Comesaña[1], Dr. F. Lusquiños[2], Dr. A. Badaoui[1], Prof. J. Pou[2]

[1] Materials Engineering, Applied Mechanics and Construction Dpt., University of Vigo, EEI, Lagoas-Marcosende, Vigo, 36310, Spain.
[2] Applied Physics Department, University of Vigo, EEI, Lagoas-Marcosende, Vigo, 36310, Spain.

Dr. S. Amorim[3,4,5], Dr. D.S. Costa[3,4], Dr. R.A. Pires[3,4,5], Prof. R.L. Reis[3,4,5]
[3] 3B's Research Group, I3Bs – Research Institute on Biomaterials, Biodegradables and Biomimetics, University of Minho, Headquarters of the European Institute of Excellence on Tissue Engineering and Regenerative Medicine, AvePark, Parque de Ciência e Tecnologia, Zona Industrial da Gandra, 4805-017 Barco, Guimarães, Portugal.
[4] ICVS/3B's – PT Government Associate Laboratory, Braga/Guimarães 4805-017, Portugal.
[5] The Discoveries Centre for Regenerative and Precision Medicine, Headquarters at University of Minho, Avepark, 4805-017 Barco, Guimarães, Portugal.

Dr. A. Solanki[6], Dr. A.L.B. Maçon[6], Dr. F. Tallia[6], Prof. J.R. Jones[6]
[6] Department of Materials, Imperial College London, South Kensington Campus, London, SW7 2AZ, UK.

*E-mail: ariveiro@uvigo.es

Keywords: laser spinning, hyaluronic acid, hydrogel, bioactive glass, lithium

Abstract

The repair of articular cartilage lesions in weight-bearing joints remains as a significant challenge due to the low regenerative capacity of this tissue. Hydrogels are candidates to repair lesions as they have similar properties to cartilage extracellular matrix but they are unable to meet the mechanical and biological requirements for a successful outcome. Here, we reinforce hyaluronic acid (HA) hydrogels with 13-93-lithium bioactive glass micro- and nanofibres produced by laser spinning. The glass fibres are a reinforcement filler and a platform for the delivery of therapeutic lithium-ions. The elastic modulus of the composites is more than three times higher than in HA hydrogels. Modelling of the reinforcement corroborates the experimental results. ATDC5 chondrogenic cells seeded on the composites are viable and more proliferation occurs on the hydrogels containing fibres than in HA hydrogels alone. Furthermore, the chondrogenic behavior on HA constructs with fibres containing lithium is more marked than in hydrogels with no-lithium fibres.

1. Introduction

Articular cartilage lesions are one of the most common joint disorders in weight-bearing joints, especially in the knee. These lesions may be associated to pain, mobility impairment, and reduced quality of life. Despite its socioeconomic impact, the repair of articular cartilage defects remains a significant challenge in orthopedic medicine due to the low regenerative capacity of this tissue [1]. The lack of self-healing response is based on its relative hypocellular and avascular structure. Defects in the cartilage slowly grow over time due to mechanical loads, and eventually may lead to long-term complications such as osteoarthritis (OA) [2]. Articular defects can be restricted to the superficial layer of the cartilage or can extend deeper, also affecting the underlying subchondral bone. Curl *et al.* reported that in 63% of 31,516 knee arthroscopies, chondral lesions were found, being a 20% grade 4 lesions (i.e. exposed subchondral bone) [3]. Subchondral defects are normally produced by the breakdown of the cartilage and the bone underneath due to a severe trauma or disease [4]. The repair of these defects is even more complicated because they require the simultaneous regeneration of cartilage and bone.

Hydrogels are a well-studied material for the regeneration of cartilage. They are three-dimensional polymer networks with hydrophilic groups or domains giving them the ability to absorb and keep a high-water content, acquire a viscoelastic shape, and large permeability. These properties facilitate the transport of drugs, oxygen, nutrients, and waste, which is of utmost relevance for tissue regeneration. Hydrogels have received widespread interest for cartilage and bone tissue engineering because of their large structural similarity to the extracellular matrix (ECM) and their porous framework, which makes possible cell transplantation and proliferation [5]. They have the ability to fill a defect, eliminating the necessity for patient-specific shaping of a scaffold [6]. Hydrogels tested for cartilage and bone

tissue engineering include natural biomaterials such as: chitosan, collagen/gelatin, alginate, fibrin, elastin, heparin, chondroitin sulfate, and hyaluronic acid and synthetic polymers such as: poly(vinyl alcohol), poly(ethylene glycol), polyglycolic acid, or poly(2-hydroxyethyl methacrylate) among others [5,7,8].

Although hydrogels have very interesting properties for cartilage and bone tissue repair, there are some problems to be addressed before they can be effectively used for that purpose. They have low mechanical stability, both in tension and compression, which makes handling and in vivo applications difficult. This low strength is related to their high-water content, and to their relatively fragile polymer network. Different methods have been applied to enhance their mechanical properties, for example, by increasing the polymer concentration, the crosslinking degree, or by using double/triple-network gels [9,10]. However, these approaches may influence the biological performance of the material, as noticed by Nicodemus *et al.* [11]. An impact on the anabolic and catabolic activity of chondrocytes encapsulated in PEG hydrogels, as well as in the type and spatial evolution of the tissue deposited was observed as a function of the crosslinking degree. Another approach consists in the reinforcement of hydrogels with woven and non-woven meshes of nano- and/or microfibres. Non-woven fibres were used to reinforce gelatin methacrylate (GelMA) hydrogels with carbon nanotubes [12], or silk hydrogels with silk microfibres [13]. Visser *et al.* showed that the stiffness of a gelatin methacrylamide (GelMA) hydrogel synergistically increased (up to 54-fold) with the reinforcement of a 3D printed network of polycaprolactone (PCL) microfibres produced by melt-electrospinning [14]. Although scaffolds based on hydrogels reinforced with micro- or nanofibres have attracted the attention of biomaterial scientists for cartilage- and bone tissue-engineering applications, there are no reports on hydrogels reinforced with bioactive glass micro- and nanofibres. One of the main reasons is their complicated production as

crystallization tends to occur during the fibre drawing (thus, reducing the bioactivity of the fibres).

Due to their biocompatibility and bioactivity, bioactive glasses are efficient implant biomaterials to replace or repair damaged tissues, especially to stimulate a more rapid bone repair [15]. Ionic dissolution products from bioactive glasses have been shown to stimulate the expression of several genes of osteoblastic cells [16]. Furthermore, the bioactivity of these materials can be enhanced by introducing therapeutic ions [17,18]. These ions not only show osteogenic and angiogenic properties, but also antibacterial or anti-inflammatory characteristics [19,20]. In particular, lithium doped glasses, as a platform for a sustained release of Li^+ ions, are interesting, especially for the regeneration of damaged bone and osteochondral tissues [21,22]. Zamani *et al.* showed that lithium, in patients treated with lithium carbonate, may preserve or enhance bone mass [23]. Clément-Lacroix *et al.* showed that oral administration of Li^+ ions enhances subchondral bone formation via activation of the canonical Wnt signaling pathway [24]. Wu *et al.* [21] fabricated lithium-containing mesoporous bioactive glass scaffolds that promoted regeneration of subchondral bone, and hyaline cartilage-like tissues compared to lithium-free bioactive glass, upon implantation in rabbit osteochondral defects. Although, the defect was filled with cartilage-like tissues, also a fibrous tissue was simultaneous deposited, and a complete restoration was not achieved.

This work aims to produce a hyaluronic acid (HA) hydrogel reinforced with non-woven 13-93 lithium-doped bioactive glass micro- and nanofibres to address the repair of subchondral defects. HA hydrogels were selected as a matrix because they are a major component of synovial fluid and glycosaminoglycans (GAGs) found in articular cartilage [25,26]. Furthermore, they have been proven to support cell proliferation and maintain the chondrogenic phenotype [27–29]. The bioactive glass micro- and nanofibres were made from the silicate 13-93 bioactive glass, and doped with lithium. The selection of this glass is based on its proven bioactivity [30], its

potential as a suitable substrate for tissue-engineered osteochondral grafts and in repairing bone defects, and as a culture medium supplement to improve the biochemical and mechanical properties of a tissue-engineered cartilage layer [31,32]. In this context, lithium was incorporated into the glass composition to act as an active ion to promote the cartilage regeneration. Bioactive glass is a good vehicle for Li^+ delivery because these ions can be incorporated into the silica network and are released as the glass biodegrades.

Bioactive glass micro- and nanofibres were produced by the laser spinning technique [33]. Once micro- and nanofibres containing lithium were obtained, their structural, chemical characteristics and dissolution behavior were determined. After that, HA hydrogels containing fibres were produced. Their swelling behavior, chemical structure and rheological properties were measured. Finally, the biological performance of these composites was evaluated. ATDC5 cell adhesion, viability and proliferation on hydrogels, as well as their chondrogenic behavior were also determined.

2. Experimental Section

2.1. Synthesis of the bioactive glass precursors and micro- and nanofibres by laser spinning.

Bioactive glass plates in the system SiO_2-Na_2O-K_2O-CaO-MgO-P_2O_5 were prepared using a melt–quench route. In this system, Li_2CO_3 was added in increasing amounts and the CaO was partially substituted. Substitutions of Ca with Li 1%, 2%, 5%, 10%, and 25% on a molar basis were performed (Table 1).

Mixtures of analytical grade SiO_2 (Prince Minerals Ltd., Stoke-on-Trent, UK) Na_2CO_3, K_2CO_3, $CaCO_3$, MgO, P_2O_5, and Li_2CO_3 (Sigma-Aldrich, Gillingham, UK) were melted in a platinum-gold crucible for 1.5 h at 1400 °C using an electric furnace (EHF 1700, Lenton, Hope Valley, UK). A batch size of approximately 200 g was used. After melting, the glasses were rapidly

quenched into deionized water. Then, the glass frit was dried at 120 °C overnight, melted again in a platinum crucible at 1300°C to pour into a graphite mold (graphite molds preheated at 500 °C), in order to make glass plates (approximated dimensions 60 x 20 mm x 10 mm). Glass plates were introduced into an oven at 500 °C during 15 min and finally were cooled down up to room temperature overnight in the same oven.

Table 1. Compositions in molar percentage of the bulk glasses used as precursor material.

	13-93-0_Li	**13-93-1_Li**	**13-93-2_Li**	**13-93-5_Li**	**13-93-10_Li**	**13-93-25_Li**
SiO_2	54.6	54.6	54.6	54.6	54.6	54.6
CaO	22.1	21.9	21.7	21.0	19.9	16.6
K_2O	7.9	7.9	7.9	7.9	7.9	7.9
Na_2O	6.0	6.0	6.0	6.0	6.0	6.0
MgO	7.7	7.7	7.7	7.7	7.7	7.7
P_2O_5	1.7	1.7	1.7	1.7	1.7	1.7
Li_2O	-	0.2	0.4	1.1	2.2	5.5

2.2. Synthesis of bioactive glass micro- and nanofibres by laser spinning

Mats of micro- and nanofibres were produced using the laser spinning technique as previously described by Quintero *et al.* [33]. A high-power CO_2 laser (Rofin Sinar DC 035) emitting a beam of infrared radiation (λ=10.6 μm) in continuous-wave (CW) mode, was focused 6 mm above the surface of the glass plates to set an irradiance of 8×10^5 W/cm^2. This laser beam was moved at 10 mm/s with regard to the glass plates. Compressed air at 10 bar was used to produce a quick elongation and cooling of a small volume of molten material, and in consequence, to produce a large quantity of micro- and nanofibres.

2.3. Synthesis of HA hydrogels reinforced with bioactive glass fibres

Hyaluronic acid (HA) hydrogels were synthetized by slightly modifying already reported procedures [34–36]. Cylindrical gels were produced by crosslinking an alkaline solution of sodium hyaluronate with divynilsulfone (DVS) in custom-made cylindrical polydimethylsiloxane (PDMS) molds (7 mm in diameter and 3 mm depth). Bioactive glass fibres were placed at the bottom of each mold to produce the composite gel. Different mass ratios of fibers to hydrogel (4/100, 10/100, 20/100) were tested. Sodium hyaluronate (700-1800 kDa, Sigma Aldrich) was dissolved into 0.2M NaOH, and stirred for approximately 1 hour at room temperature to give a 4% (w/v) solution. 120 μL of this solution were transferred to each mold to produce one cylindrical gel. Then, DVS (Sigma Aldrich) was added (HA/DVS weight ratio 1:1) for the crosslinking reaction with the hydroxyl groups of HA. The reaction was performed at 25 °C for 1 h. Although DVS cross-linked HA shows good cytocompatibility, as confirmed in different works by cell viability assays [37] or histological analyses [38], hydrogels were washed to remove unreacted DVS and/or NaOH from the gels. The product was washed 12 h into 100 ml DI water, equilibrated into 100 mL TRIS buffer solution (pH=7.4), and finally washed into 100 mL DI water for 12 h.

Solutions of sodium hyaluronate and DVS were initially sterilized by filtration using 0.22 μm syringe filters. Bioactive glass micro- and nanofibres were sterilized by exposing the fibres to 254 nm ultraviolet (UV) radiation during 30 mins. Hydrogels were synthetized into a laminar flow cabinet to guarantee the sterile conditions of the final gels. The crosslinking of the HA hydrogels with DVS was confirmed by FTIR-ATR analyses on lyophilized hydrogels with and without glass fibres.

2.4. Physicochemical characterization of fibres and hydrogels

2.4.1. Morphology of fibres

The morphology of the fibres was determined using FESEM (JEOL JSM-6700f). After synthesis, the collected fibres were characterized without further post-processing. Samples

were mounted on SEM stubs with the aid of two-sided adhesive carbon discs (Agar Scientific, Stansted, UK). Samples were analysed at an operating voltage of 5 kV.

2.4.2. Chemical composition of fibres

The compositions of the precursor glasses and the fibres obtained from them were analysed by XRF spectroscopy (Siemens SRS3000) under the same conditions of analysis.

2.4.3. pH and ion release from the fibres in Tris buffer

The dissolution products from the bioactive glass fibres were studied in Tris-buffered solutions in which the pH was adjusted to 7.4 with 1M HCl. The preparation of Tris buffer solution was performed according to the procedure described by Mneimne *et al.* [39], and the specimens were prepared in triplicate.

Bioactive glass fibres were incubated in Tris-buffer solution using a ratio of 75 mg glass to 50 mL of buffer solution in an airtight polyethylene container as described in [40]. Samples were placed in an incubating orbital shaker held at 37 ± 1°C, at an agitation rate of 120 rpm, for 1, 2, 4, 8, 24, 72 and 168 h. At these time points, the pH of the solution was recorded (Oakton pH 11 series pH), and 0.5 mL of supernatant was removed and replaced by 0.5 mL fresh Tris-buffer solution. The 0.5 mL solutions were analysed by inductively coupled plasma optical emission spectroscopy (ICP-OES; Optima 5300DV, Perkin Elmer), after dilution 1:10 with 1% w/v nitric acid, to determine the amount of Si, Ca, K, Na, Mg, P and Li in the Tris solution after glass immersion. The value obtained for each ion was compared to the value obtained for the blank samples (only Tris).

After removing the samples from the shaker, fibres were collected by filtration (5-13 μm particle retention, VWR International, Lutterworth, UK). They were immediately washed with DI water, and then with acetone to avoid any further reaction; finally, they were dried at 37 °C during 24 h for further analyses. The initial mass of the glass fibres and their mass after immersion in Tris-buffer solution (dried samples) was measured (accuracy of 0.01 mg) to

determine the mass change. FTIR-ATR (Nicolet i510, ThermoScientific) and SEM (Philips XL 30) analyses were also performed on the dried glass fibres.

2.4.4. Zeta potential of fibres

The zeta potential of the bioactive glass micro- and nanofibres was determined with the SurPASS electrokinetic analyzer (Anton Paar GmbH, Graz, Austria) using a cylindrical cell developed for the measurement of fibrous samples. The principle for the zeta potential determination of the fibres with the SurPASS analyzer is based on the measurement of the streaming potential [41–43]. The pH dependence of the zeta potential (in a range of pH from 4 to 10) was investigated with a background electrolyte of 1 mM NaCl solution.

2.4.5. Young's modulus of the fibres

The preparation of the samples for the AFM characterization was as follows. A drop of 0.05% (w/v) solution of poly-L-lysine (PL, molecular weight 30000-70000 kDa, Sigma Aldrich) was applied on the surface of a freshly cleaved mica. After incubation for 15 minutes, the surface was rinsed with a 0.15 M NaCl solution, washed with DI water and dried with nitrogen. Finally, a drop of DI water was applied to the surface of the PL-coated mica, and microfibres (only, 5 microfibres were deposited onto the mica substrates to avoid any interaction among them) were deposited on this drop. Prepared samples were dried at room temperature before being examined by the AFM.

The glass fibres were analysed using a BioAFM (JPK NanoWizard® 3, Germany) and TAP525 probes (Bruker, Germany) presenting a typical spring constant of 200 N/m, a resonance frequency 525 kHz and a tip radius of 12 nm. Each probe was calibrated using contact-based methodology (onto the mica surface), yielding individual prove specific sensitivity and resonance frequency. Nanoindentation force curves of the glass fibres were used to calculate the fibres' Young moduli using the Hertz model. A paraboloid tip shape was selected due to the very low indentations (~1nm) used. All the AFM experiments were executed under JPK

Advanced Quantitative Imaging (QI) mode, which allows the mechanical properties to be calculated and the topography of the fibres to be recorded with the same dataset.

2.4.6. Swelling of hydrogels

HA-DVS hydrogels (with and without fibres) were immersed into distilled water at 25 °C to determine their swelling behavior as a function of time. Experiments were performed in DI water because the swelling ratio of HA hydrogels reaches the maximum attainable swelling in this system as observed by Zawko *et al.* [44]. The swelling ratio (SR) was calculated according to Eq. (1):

$$SR = \frac{W_s - W_d}{W_d} \cdot 100 \quad (1)$$

where W_s (in mg) is the swollen weight of the hydrogel, and W_d (in mg) is the dry weight of the hydrogel. The dry weight of the hydrogel was determined from lyophilized hydrogel samples.

2.4.7. Rheological characterization of hydrogels. Halpin-Tsai equations

The mechanical properties of HA-DVS hydrogels were characterized by oscillatory rheology studies using cone-plate geometry at 37 °C using Malvern Kinexus Rotational Rheometer (Malvern, UK). Paraffin oil was poured around the perimeter of the sample (but, mixing with the sample was avoided), and the insulating chamber was closed to prevent the evaporation of water from the sample.

The aim of the rheological measurement was the determination of the G' and G" values (the elastic modulus and viscous modulus, respectively) as a function of the mass of fibres incorporated to the hydrogels. A fresh sample was used for each measurement. Each experiment was performed in triplicated. Only the average results are reported here. These results have been compared with the theoretical predictions given by the Halpin-Tsai equations (Eqs. B.1-B.4, Appendix B) [45].

2.5. Biological characterization of fibres and hydrogels

2.5.1 Cell Culture

Chondrogenic ATDC5 cells were cultured in Dulbecco's Modified Eagle Medium:Nutrient Mixture F-12 (DMEM / F12) (Invitrogen, USA) supplemented with 10% heat-inactivated fetal bovine serum (FBS; Biochrom AG, Germany) and 1% antibiotic/antimyotic solution (final concentration of penicillin 100 units/mL and streptomycin 100 mg/mL; Gibco, UK). Cells were cultured in a 5 % CO_2 incubator at 37 °C. Confluent ATDC5, were harvested, seeded and cultured for 7, 14 and 21 days, at a density of 150,000 cells/cm^2 on the HA hydrogels without fibres (NF) and on HA hydrogels with fibres of the compositions 13-93-0_Li (fibres without lithium), 13-93-5_Li, and 13-93-10_Li. Briefly, the seeding was performed on the top of the gels, with a concentrated drop of 50 µL. After 4 h of adsorption, the wells were fulfilled with culture medium.

2.5.2 Live/Dead cell staining

Viability of cells was tested by a Live–Dead assay performed 7, 14 and 21 days, post culture. The cell–hydrogel constructs were washed three times with PBS and then a 1 mL aliquot of the assay solution containing 2 µL of Calcein-AM (Invitrogen, USA) and 0.6 µL of Ethidium Homodimer-1 (Sigma-Aldrich, USA) in PBS, was pipetted onto each cell–gel construct. The constructs were observed using Confocal laser scanning microscope (Leica TCS SP8) with 488 nm (green, Calcein AM) and 633 nm lasers (red, EthE-1).

2.5.3 Cell viability and proliferation (MTS assay and DNA content)

The ATDC5 viability for each culturing time was determined using the Cell Titer 96® Aqueous One Solution Cell Proliferation Assay (Promega, USA). This assay is based on the bioreduction of a tetrazolium compound, 3-(4,5-dimethylth-iazol-2-yl)-5-(3-carboxymethoxyphe-nyl)-2-(4-sulfofenyl)-2H-tetra-zolium (MTS), into a water-soluble brown formazan product. NADPH or NADH production accomplishes this conversion by the dehydrogenase enzymes in

metabolically active cells. The absorbance was measured at 490 nm using a microplate reader (Synergie HT, Bio-Tek, USA), being related to the quantity of formazan product.

Cell proliferation was quantified by the total amount of double-stranded DNA along the culturing time. Quantification was performed using the Quant-iT PicoGreen® dsDNA Assay Kit (Invitrogen, Molecular Probes, Oregon, USA), according to the manufacturer's instructions. Briefly, ATDC5 were lyzed by osmotic and thermal shock and the supernatant was used for the DNA quantification assay. A fluorescent dye, PicoGreen, was used because of its high sensitivity and specificity to double-stranded DNA. The fluorescence of the dye was measured at an excitation wavelength of 485/20 nm and at an emission wavelength of 528/20 nm, in a microplate reader (Synergie HT, Bio-Tek, USA).

Triplicates were carried out for each sample and per culturing time. The DNA concentration for each sample was calculated using a standard curve (DNA concentration ranging from 0.0 to 1.5 $mg.mL^{-1}$) relating the quantity of DNA with the fluorescence intensity.

2.5.4 Total sulfated GAGs quantification

Quantification of sulfated GAGs was performed by their solubilization through exhaustive proteolitic digestion. Papain fully solubilize GAG, by cleaving the core protein. The hydrogels were incubated at 60 °C for 3 h, in a Papain digestion solution containing 200 mM of phosphate buffer containing 1 mM EDTA (pH 6.8) (Digestion buffer), with 25 mg of papain and 48 mg of n-acetyl cysteine (per 50 mL of digestion buffer). After proteinase digestion, sulfated GAGs were quantified by BlyscanTM Sulfated Glycosaminoglycan Assay Kit (Biocolor Ltd, UK), according to the manufacturer's instruction.

2.5.5 Protein extraction and Western-blotting

Hydrogels were washed twice with phosphate-buffered saline, cells were lysed in lysis buffer (100mM Tris, pH7.6, 4 % sodium dodecyl sulfate and 0.1M DTT) on ice for 30 min, followed by heating step at 95 °C (10 min) and centrifugation at 12,300 g for 10 min at room temperature. The protein concentration in all samples was measured using Micro BCA™ Protein Assay Kit

(Pierce, Thermo Scientific, USA). Equal protein concentrations (60 µg) were loaded on a 9% polyacrylamide gel. After gel electrophoresis at 150 V, proteins were blotted onto a nitrocellulose membrane (Amersham Biosciences, UK) using Pierce Power station according to manufacturer's instructions. Membranes were then blocked in blocking buffer (5 % milk, 1 % BSA, 1 % Tween-20 in TBS-T) 30 min at room temperature. After blocking, membranes were rinsed and probed for 1 h with rabbit polyclonal anti-alpha actin (1:1000, ab5694, Abcam) and mouse anti-aggrecan (1:1000, MA3-16888, ThermoFisher) in blocking buffer, followed by three washes with TBS-T and then incubated with an anti-rabbit (Sigma-Aldrich, USA)/anti-mouse (Vector, UK) alkaline phosphatase-conjugated secondary antibody at 4 °C for 16 h. Protein bands were visualized using colorimetric AP development kit (Bio-Rad, Netherlands).

2.5.6 Statistical Analysis

The normality of the data was evaluated using Shapiro−Wilk test. When the data did not follow a normal distribution a Kruskal Wallis followed by Mann-Whitney tests were performed (DNA and MTS), with a significance level of 99 % (p<0.001).

3. Results and discussion

3.1. Micro- and nanofibres synthesis and physico-chemical characterization

Mats of micro- and nanofibres, with a cotton-like appearance (Figure 1a), were produced using laser spinning technique from plates of 13-93 bioactive glass. They form a disordered mesh of intertwined fibres with diameters ranging from tens of nanometers to micrometers, and with lengths of several millimetres (even in the centimetre range in some cases). Some glass dust was observed on the fibres because of the condensation of vapours produced during the partial vaporization of glass during laser spinning. The estimated production rate of glass fibres during the laser spinning process was around 8.4 mg of glass fibres per mm of precursor glass plate

irradiated by the laser beam (or equivalently a mass production rate of 1.4 mg/s, a value much higher than in electrospinning).

The compositions of the fibres were close to the measured compositions of the bulk glass precursor material and to the theoretical compositions (Table 2). This is in agreement with previous works on laser spinning which showed that the process does not significantly change the composition of the bioactive glasses [33].

Table 2. Compositions in molar percentage of the glass plates and the fibres measured with XRF.

	13-93-0_Li (Theoretical)	**13-93-0_Li (Bulk)**	**13-93-0_Li (Fibres)**	**13-93-25_Li (Theoretical)**	**13-93-25_Li (Bulk)**	**13-93-25_Li (Fibres)**
SiO_2	54.6	55.94	57.04	54.6	56.39	57.16
CaO	22.1	21.14	22.04	16.6	17.43	18.14
K_2O	7.9	8.01	7.87	7.9	7.79	7.58
Na_2O	6	5.85	4.58	6	5.02	4.55
MgO	7.7	7.32	6.97	7.7	6.74	6.52
P_2O_5	1.7	1.74	1.5	1.7	1.53	1.38
Li_2O	-	-	-	5.5	5.10	4.67

The composition of the glass fibres plays an important role in the final appearance and fibre diameter (Figure 1b-g). The fibre diameter decreased as lithium content increased, and they became cleaner. This is explained due to the influence of the lithium content on the viscosity [46] and surface tension [47] of the glass melts; both are key factors influencing the fibre diameter in laser spinning [48].

The topographical analysis of the fibres with SEM and AFM reveals that fibres maintain a well-defined cylindrical morphology (Figures 1b-g and 2a). Furthermore, their surface is quite smooth (Figure 2a), with and average roughness of R_a=1.86±0.76 nm (and a root mean square deviation of the roughness profile R_q=2.34±0.96 nm).

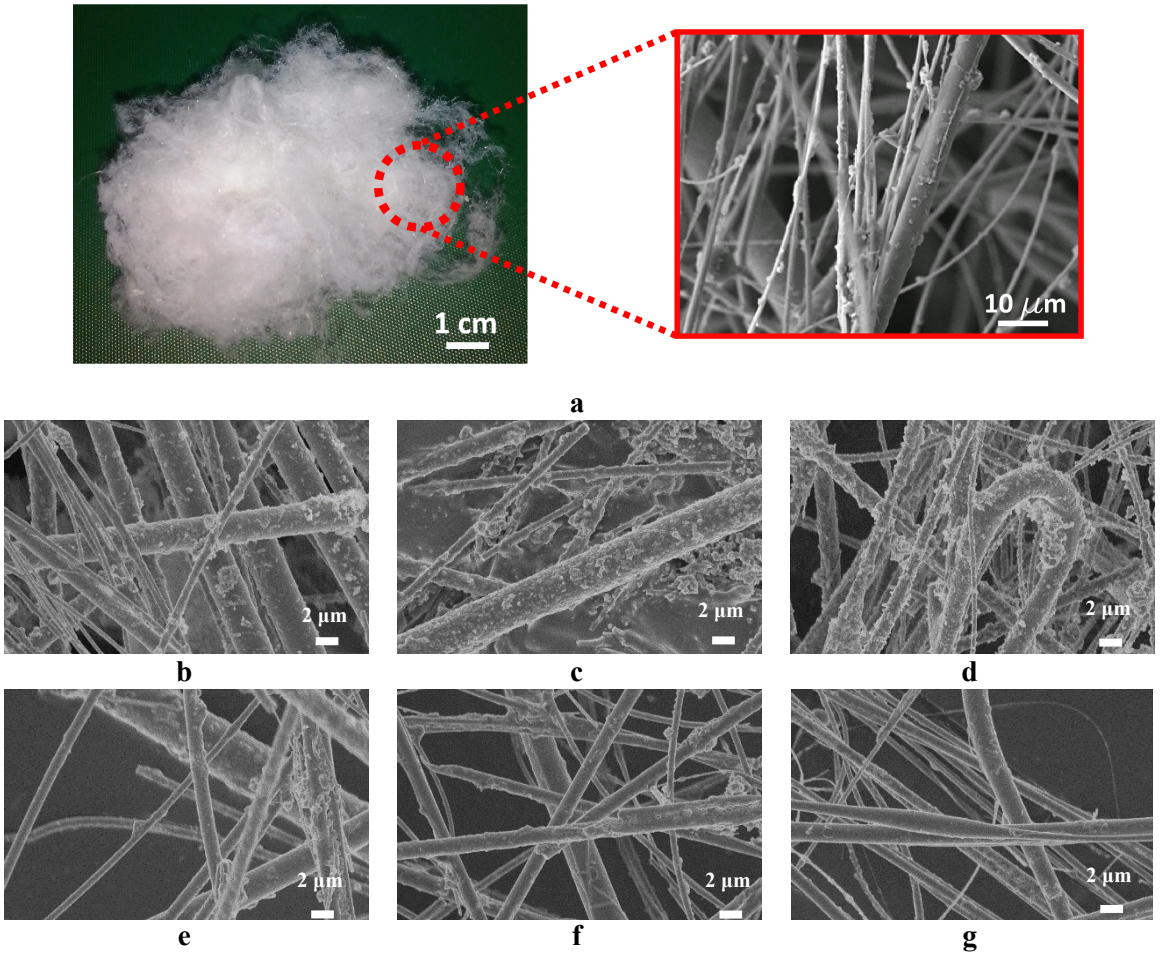

Figure 1. a) Optical micrograph and a detail obtained by electron microscopy of the mats of bioactive glass micro- and nanofibres produced by laser spinning. SEM micrographs of micro- and nanofibres produced from glasses with different lithium content: b) 13-93-0_Li, c) 13-93-1_Li, d) 13-93-2_Li, e) 13-93-5_Li, f) 13-93-10_Li, and g) 13-93-25_Li.

The Young's modulus of the fibres was measured with an AFM to study its influence on the mechanical properties on the hydrogel composites. The measurements reveal an influence of the lithium content on the stiffness of the fibres. The increased lithium content makes the glass fibres stiffer, shown by the Young's modulus increasing from approximately 3.85 GPa for the fibres without lithium (13-93-0_Li) up to 18.85 GPa for the fibres with the largest amount of lithium (13-93-25_Li) (Figure 2b). The replacement of large ions as calcium by small ions as lithium (with a high-field strength) may distort the glass network and increases the Young's modulus [49,50].

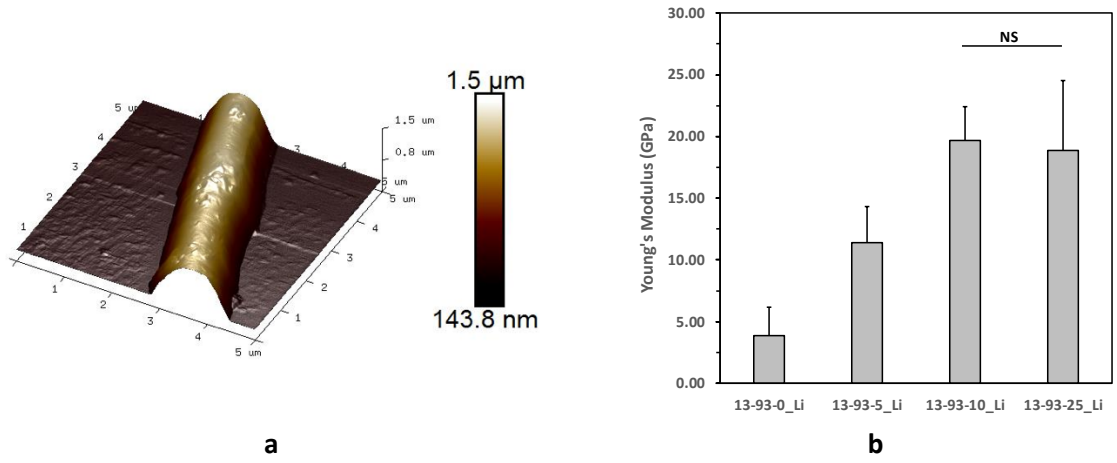

Figure 2. a) Three-dimensional view of the signal given by the AFM height sensor of a fibre with 1.31 µm in diameter (Glass composition 13-93-0Li). b) Young's modulus for glass fibres as a function of the composition. All the samples showed a significantly different Young's modulus, with the exception of those marked with NS.

Cumulative concentrations of Si, Ca, P, and Li released from the 13-93-Li-derived fibres during incubation in Tris buffer solution are shown in Figures 3a-d. Silica release gives an idea on the overall degradation of the fibres because it is the glass network former. Maximum cumulative Si levels of 65.92 ± 0.10 ppm for the 13-93-0_Li fibres, and 69.73 ± 0.15 ppm for the 13-93-25_Li fibres were found after immersion for 24 h. These values are higher than those reported for lower surface area scaffolds of the same glass; for example, Hoppe *et al.* reported values of 30 ppm for macroscopic scaffolds of 13-93 glass after immersion for 21 days [51]. Similar values to those reported in this work were found by Qazi *et al.* [52], where Si release after immersion for 24 h reached values of ~80 ppm for 45S5 Bioglass® (average particle size of 3.6 ± 0.8 µm) and for 13-93 (average particle size of 4.8 ± 1.6 µm) glass particles. The larger surface area of the micro- and nanofibres substantially promotes the degradation of the fibres. It was estimated that the overall degradation of the fibres (for all the glass compositions), expressed in terms of mass loss, was about 35% after immersion for 7 days in Tris buffer solution.

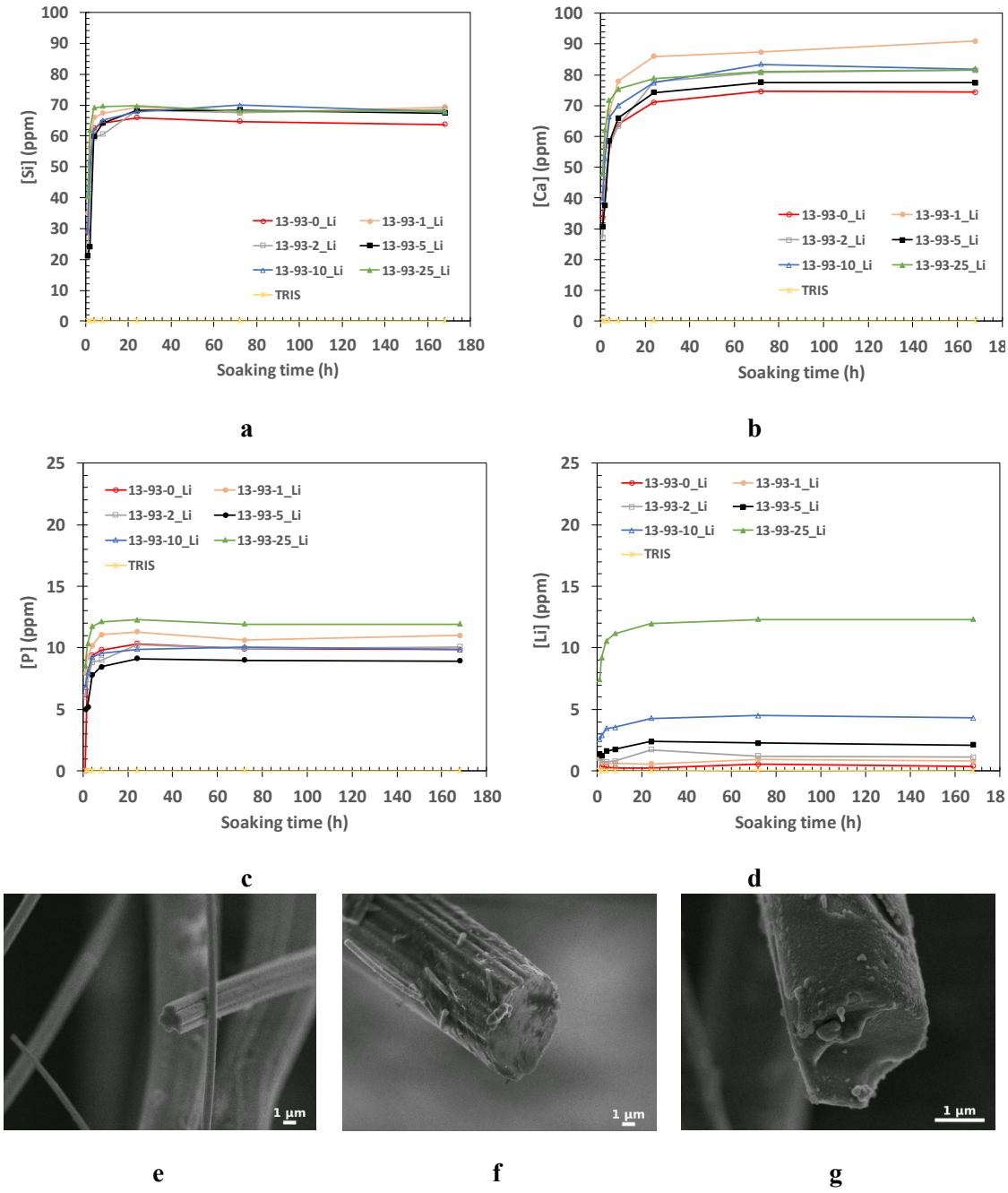

Figure 3. Release of accumulated a) Si, b) Ca, c) P, and d) Li from the 13-93-Li-derived fibres in Tris buffer solution. SEM images of the glass fibres after incubation in Tris for 7 days for the compositions e) 13-93-0_Li, f) 13-93-5_Li, and g) 13-93-25_Li respectively.

ICP–OES data show that, as expected, the Li release was higher in samples with higher lithium content, with an initial burst in the first 24 h followed by a more sustained release. Li was continuously released from the fibres over the first 24 h, reaching a maximum cumulative value of 11.97 ± 0.05 ppm after immersion for 24 h for the 13-93-25_Li glass fibres. The concentration of Li released by these 13-93-25_Li glass fibres was slightly higher than the

recommended therapeutic ranges established for humans (between approximately 4.2 and 8.3 ppm) [23]. However, values for fibres with a lower lithium content are within the recommended range. It is worth to mention that there is some discussion about the maximum values for lithium doses which can produce deleterious effects [24].

Notice that after an initial burst of lithium, the ion release after 24 hours continues but with a decreasing release rate. This can be due to a change of the release mechanisms as the fibres are not fully degraded after 7 days immersed, and then continue to dissolve and supply active ions (see Figs. 3e-g). Then, lithium release proceeds as the glass matrix is degraded, but at a slower rate. This would guarantee a continuous supply of lithium to the damaged area.

Other ions in the glass fibres, such as Ca or P exhibited a similar dissolution behavior; however, there is no linear relation between the amount of lithium added to the precursors glasses and the release of these ions. As stated by Kargorzar et al, the introduction of an alkali ion of small ionic radius (such as Li+) would result in a more compact network, and in a decrease in the dissolution rates [19]; however, the current contradictory results could be attributable to the mixed alkali effect which influences the ion release behavior in silicate glasses with mixed alkali compositions [53,54]. In these cases, the ion release is reduced and shows a non-linear behavior as compared to glasses containing only one alkali oxide [55]. The dissolution experiments do not show a significant decrease in the cumulative value of P and Ca. This suggests that calcium phosphates did not nucleate on the surface of the fibres, as further corroborated by FTIR and SEM characterization.

Zeta potential of the fibres (measured in 1mM NaCl dissolution) showed negative values at acidic, neutral and basic pH values (Fig. C.1, Appendix C). Zeta potential increased with the lithium content. Values of -28.0±0.4 mV, -46.0±0.8 mV and -42.0±1.2 mV were measured for the 13-93-0_Li, 13-93-10_Li and 13-93-25_Li respectively. These values were observed to increase with the dissolution time. The dissolution of network modifier cations (accompanied by surface rearrangements), and their impact on the electrochemical double layer caused this

increase [42]. This is in agreement with the weight loss observed during the dissolution experiments. Weight loss after 7 days in Tris solution was 36.0±2.9%, 39.6±4.0% and 40.9±1.8% for the 13-93-0_Li, 13-93-10_Li and 13-93-25_Li respectively.

FTIR spectra of glass fibres before and after immersion for 7 days looked similar, and no difference was found irrespectively of the lithium content (Figure 4). Formation of a silica rich layer after immersion was detected in all the cases [56]. FTIR spectra showed distinctive absorption bands at ~450 cm^{-1} (symmetric stretching, ν_{sym}(Si–O–Si)), ~760 cm^{-1} (bending mode δ(Si–O–Si)), ~930 cm^{-1} (SiO_{NBO} shoulder, associated to glass network modifiers), and ~1060 cm^{-1} (asymmetric stretching, ν_{asym}(Si–O–Si)) [56,57]. After immersion in Tris, no differences were also seen between fibres with different lithium content (Figure 4b). The FTIR spectra showed a decrease in the band associated with modifying cations (SiO_{NBO}), as the modifiers are released from the glass and accumulated in the Tris solution [57]. On the other hand, the band at ~1060 cm^{-1} (ν_{asym}(Si–O–Si)) became more prominent, suggesting the formation of a silica rich layer [56]. An additional shoulder at ~1220 cm^{-1} appears after incubation. This band is typically seen in vitreous silica [51].

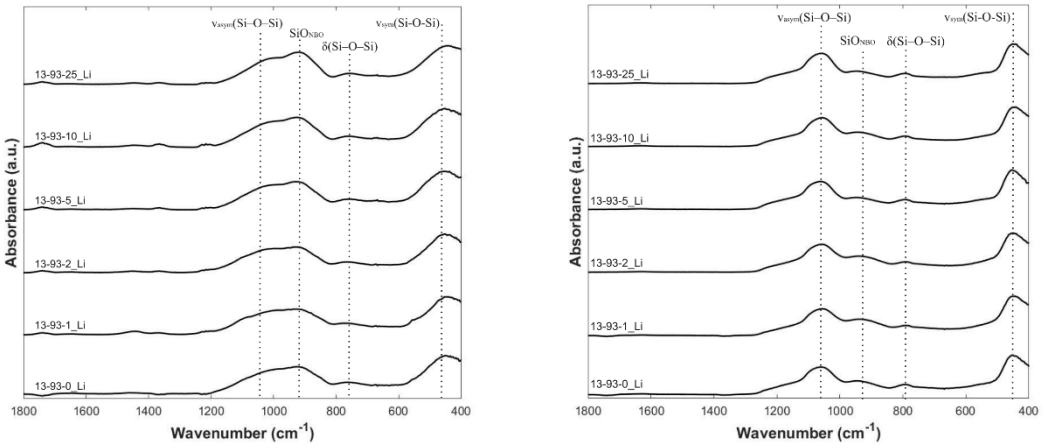

Figure 4. ATR-FTIR spectra of the glass fibres a) before, and b) after incubation in Tris buffer solution.

Formation of apatite was demonstrated by immersion tests of glass fibers into SBF (using the procedure described in Ref. [40]). As demonstrated (see Fig. A.1, Appendix A), apatite nucleates on the surface of the glass fibers without lithium after 3 days immersion in SBF, while in those lithium-containing fibers it nucleates after 7 days immersion in SBF. This delay in apatite nucleation could be an indication of a more compact network in lithium-containing glasses. Delayed apatite formation in SBF (compared to the no-Li glass), and the fact that it is not formed in Tris buffer, is good for cartilage regeneration, as we do not want apatite to form in the cartilage. However, this slow apatite formation in SBF may enable bonding to subchondral bone which could aid to anchor the hydrogel.

SEM images in Figure 3d-f show the aspect of the glass fibres after incubation in Tris for 7 days. Prior to incubation (Figure 1b-g), the fibres looked to have similar morphology, and some glass dust produced during the laser spinning process was seen adhering to the surface of the fibres. After incubation in Tris for 7 days, the glass dust was mostly removed. A thin layer of precipitate was observed, mainly in the fibres with higher lithium content (see Figure 3g). The dissolution of the fibres, especially for those with low lithium content (see Figures 3e and 4f) seems to occur by the delamination of some strips away from the surface of the fibres. Grooves along the length of the fibres are clearly observed as a result. The mechanisms involved in this process have not been observed during the degradation of typical bioactive glasses, such as 45S5, and require further analyses to determine its origin.

3.2. Hydrogel synthesis and properties

HA hydrogels reinforced with bioactive glass fibres were synthetized in cylindrical molds (see Figure 5a-c). The utilization of lithium doped or non-doped fibres did not affected the hydrogel synthesis; therefore, we have only characterized hydrogels without lithium to make the analysis clearer. Synthetized hydrogels have a well-defined cylindrical morphology, which remained unaltered after swelling (Figure 5c).

Hydrogels were reinforced with a mass ratio of fibres to hydrogel of 4/100, 10/100, 20/100 (absolute mass of fibres into the hydrogel: 0.2, 0.5, 1 mg).

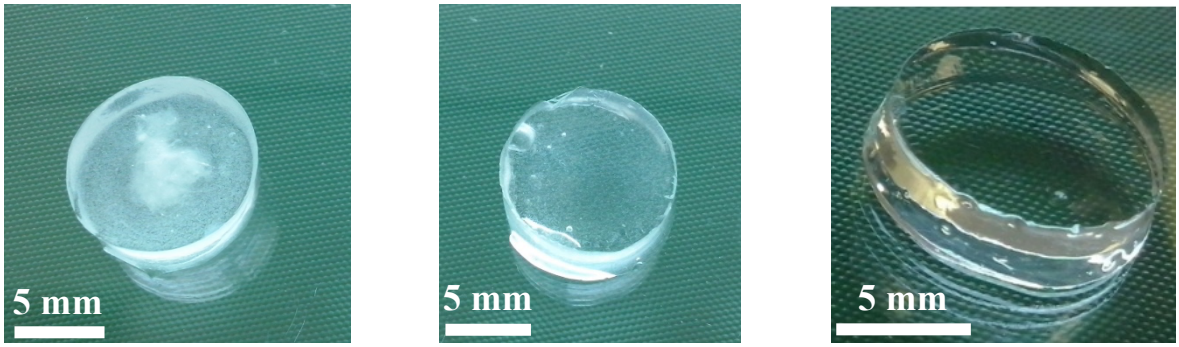

Figure 5. HA hydrogels crosslinked with divinyl sulfone a) with fibres (composition: 13-93-0_Li), b) without fibres, and c) without fibres swollen in DI water.

FTIR spectra for lyophilized HA hydrogels with different amounts of fibres (and for the sodium hylauronate) were acquired to confirm the crosslinking of HA with DVS (Figure 6a). Several bands associated to the HA appear at 3385 cm^{-1} (hydrogen-bonded O-H and N-H stretching vibrations), 2897 cm^{-1} (C-H stretching vibration), 1611 and 1402 cm^{-1} (C=O asymmetric, and C-O symmetric stretching vibrations), 1651 cm^{-1} (amide I, C=O stretching vibrations), 1560 cm^{-1} (amide II, N-H bending vibration), and 1043 cm^{-1} (C-OH group) [58,37]. Two peaks appear in the crosslinked gels at 1287 and 1120 cm^{-1}. They are related to the C-O and S=O stretching modes associated with the HA-DVS bonding, , thereby confirming that HA has been crosslinked with DVS [59]. No significant differences were found between the hydrogels with or without fibres. This suggests that the presence of the fibres does not modify the chemical structure of the hydrogel.

Swelling studies were performed on the HA hydrogels to characterize the response of the samples within an aqueous environment, an important issue for 3D cell culture and *in vivo* implantation. Therefore, the swelling ratio for hydrogels with different amount of fibres was determined as a function of the time (Figure 6b). The swelling ratio increases with time up to a point (around 8 h) where hydrogels were fully swollen. A significant change in the weight of

hydrogels did not occur for the subsequent time points. The addition of a small amount of fibres to the hydrogels (0.2 and 0.5 mg of fibres, i.e. in a 4/100, and 10/100 ratio) decreased the swelling ratio as compared to the gels without fibres; however, a higher increment of fibres (1 mg, i.e. i.e. in a 20/100 ratio) increased substantially the swelling ratio, up to a 590% after 24 hr. The relation between the swelling behavior and the amount of crosslinking has been extensively studied [60]. Therefore, these results suggest that the increment of the fibre content in the HA reduced the crosslinking degree, and increased the swelling of hydrogels. A maximum amount of fibres around 0.2-0.5 mg (4/100-10/100 ratio) did not significantly affect the swelling ratio (Figure 6b). Therefore, HA hydrogels with a maximum amount of 0.5 mg of fibres (10/100 ratio) were used for the biological characterization to avoid an excessive swelling.

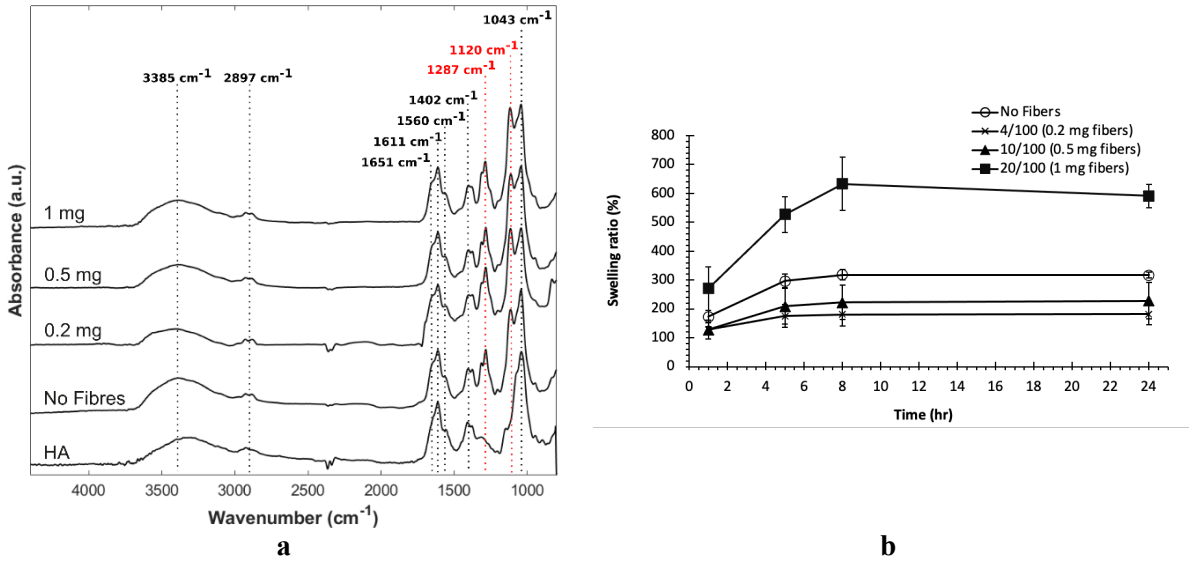

Figure 6. a) FTIR spectra of sodium hyaluronate (HA) and HA hydrogels crosslinked with DVS, with and without fibres (composition: 13-93-0_Li), and b) swelling ratio of HA hydrogels without and with fibres (composition: 13-93-0_Li; mass ratio fibres to hydrogel 4/100, 10/100, 20/100; absolute mass of fibres into the hydrogel: 0.2, 0.5, 1 mg) as a function of the immersion time in DI water.

Oscillatory rheology was performed to characterize the mechanical properties of the HA hydrogel. The storage G' (elastic response), loss modulus G" (viscous response), complex

viscosity η*, and loss tangent $\tan\delta$ were determined for HA hydrogels with different percentages of fibres (Figure 7, and Table 3). The mechanical spectra for all the hydrogels show that the elastic modulus G' was one or two orders of magnitude higher than the viscous modulus G''; furthermore, G' was almost independent of the frequency, and tan δ is in a range of 0.001-0.01. These values correspond to strong gels.

The addition of fibres to the hydrogels increased the elastic modulus from G'=1851±285 Pa (hydrogels without fibres) up to G'=6759±293 Pa (hydrogels with 0.5 mg of fibres, i.e. 10/100 ratio), at 1 Hz. A high addition of fibres slightly reduces the mechanical response (e.g. reduced up to G'=5730±368 Pa at 1 Hz, for hydrogels with 1 mg of fibres, i.e. 20/100 ratio) in agreement with the swelling results (Figure 6b). The elastic modulus of the hydrogels was up to three times higher when fibres were incorporated. The linear viscoelastic regime decreases with the incorporation of fibres into the hydrogel. The addition of 0.2 mg (4/100 ratio) of fibres into the hydrogel reduced the linear regime from a 25% strain (hydrogels without fibres) up to 10% strain. Subsequent increments of fibres reduced this trend up to 2% strain (0.5 mg of fibres; 10/100 ratio) and 1% strain (1 mg of fibres; 20/100 ratio), thus also confirming the reduction in crosslinking density with the addition of glass fibres.

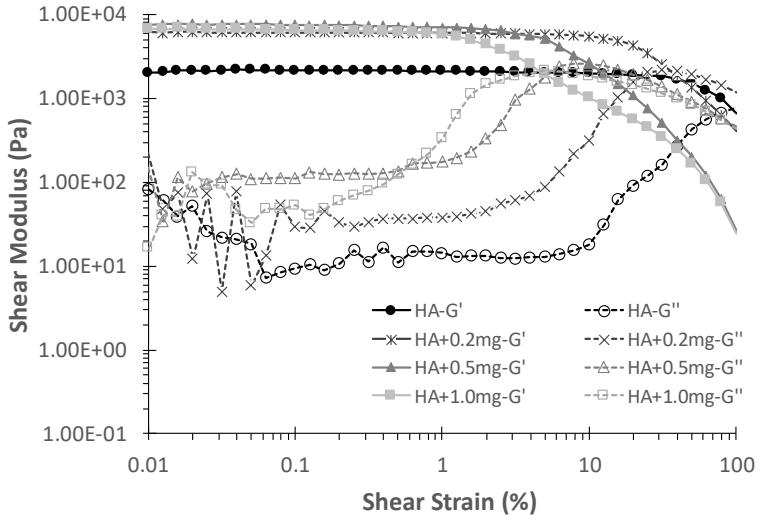

Figure 7. Strain sweep (at 1 Hz) for HA hydrogels crosslinked with DVS and different amounts of fibres (composition: 13-93-0_Li).

Table 3. Viscoelastic properties for HA hydrogels with different amount of fibres (composition: 13-93-0_Li) at a frequency of 1 Hz. Theoretical prediction of G' (using the Halpin-Tsai model) is included.

	Fibre/HA mass ratio	Viscoelastic properties @ 1 Hz				Theoretical prediction (Halpin-Tsai)
		G' (Pa)	G'' (Pa)	η* (Pa·s)	tan δ	E_c (Pa)
HA	0	1851±285	34.49±3.4	371.4±63.2	0.011±0.000	-
HA+0.2 mg fibres	4/100	5760±15	47.7±2.2	916.8±2.5	0.009±0.000	3394.2
HA+0.5 mg fibres	10/100	6759±293	155.1±47.8	1076.0±46.7	0.018±0.000	5708.9
HA+1.0 mg fibres	20/100	5730±368	20.2±17.9	912.1±58.5	0.006±0.000	9566.8

The elastic modulus of the hydrogels reinforced with fibres was calculated using the Halpin-Tsai equations (Eqs. B.1-B.4, Appendix B). These equations predict an elastic moduli E_c for the reinforced hydrogels in the same order of magnitude that those obtained for G' in the rheological experiments (Table 3). The calculated value for hydrogels with 0.5 mg of fibres (10/100 ratio) was E_c=5708.9 Pa, while the measured elastic modulus was G'=6759±293 Pa (Figure 7, and Table 3). The discrepancy between the experimental and theoretical results (G' vs E_c) was largest for the hydrogels with 1.0 mg (20/100 ratio) of glass fibres. This can be attributable to the reduction in crosslinking density with the increment of fibres into the hydrogels. From this analysis, it is concluded that the large aspect ratio of the fibres produced by laser spinning is responsible (through the ζ parameter described in Eq. B.1), at a large extent, for the increment in the elastic modulus of the composite hydrogel/fibres.

We have checked the variation of the mechanical properties of hydrogels with time (see Fig. C.2, Appendix C). It is observed that these are slightly reduced after 21 days; however, the hydrogels with fibers show better mechanical properties than those hydrogels without fibres.

3.3 Biological characterization of hydrogels reinforced with fibres

3.3.1 Effects of HA hydrogel composition on ATDC5 cells adhesion, proliferation and viability

ATDC5 chondrogenic cell line, a derived mouse teratocarcinoma cells, has been extensively studied and reported to reproduce multi-steps of chondrocyte differentiation [61]. Herein, it was used as an *in vitro* model to evaluate the chondrogenic potential of the constructs. After the seeding of cells on the top of the hydrogels, proliferation and viability of ATDC5 were followed for 7, 14 and 21 days. The scaffolds were stable during the 21 day culture period. Live/Dead assay (Figure 8) shows a qualitative evaluation of viable cells seeded on the constructs. At day 7, a lower number of adhered cells were visible on HA hydrogels without fibres (NF), and a high number of dead cells was observed. On the scaffolds with glass fibres; the number of cells adhered decreased as lithium content of the fibres increased. This result was confirmed by quantitative analysis of cell viability and proliferation, MTS assay and DNA quantification (Fig. C.3, Appendix C). However, on the latter time points (i.e. 14 and 21 days), a large number of cells are visible in all the constructs, being a green monolayer of cells highlighted on the microscopy images, at 21 days (Figure 8).

From the Live/Dead assay (Figure 8), it is noticed that, for 7 and 14 days of culture, the density of cells was quite different for each hydrogel. As reported by Ustun *et. al.* [62], the presence of nanofibres provides a favourable microenvironment for ATDC5 attachment and proliferation. Yunos *et al.* described that chondrocyte cells showed better results, on proliferation, on Bioglass scaffolds containing poly-DL-Lactide (PDLLA) nanofibres, when compared to those without fibres [63]. Our results follow the same trend, being ATDC5 more proliferative on the constructs containing glass nanofibres (sample 0_Li) (Fig. C.3, Appendix C). This result can be also related to the stiffness of the hydrogel, or to the ion release from the bioactive glass fibres.

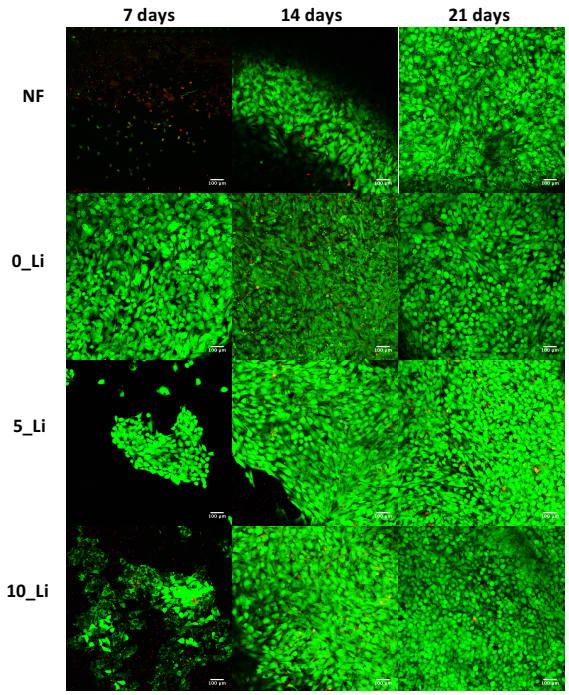

Figure 8. Live/Dead assay of ATDC5 seeded on NF, 0_Li, 5_Li and 10_Li scaffolds for 7, 14, and 21 days. Green = Live cells (Calcein-AM); Red = Dead cells (EthD1). (scale bar = 100 μm).

On the other hand, the lithium content of these fibres showed also, to have a role on the chondrogenic cells' viability and attachment. This effect is more visible on the first 7 days of culture, being the cell density lower as we increase the lithium content of the fibres (Figure 8 and Figure C.3 -Appendix C-). In fact, the effect of lithium on the differentiation of human mesenchymal stem cells into chondrogenic cell lineages, in chondrogenic cultures, has been described, and the production of cartilage mass rich in GAG was reported [64]. Specific cartilage markers were evaluated to better understand the relationship between Li content and the ATDC5 chondrogenic phenotype on the hydrogels reinforced with fibres.

3.3.2 Cartilaginous Matrix Deposition - sulfated glycosaminoglycans' (sGAG) production

Sulfated glycosaminoglycans' (sGAG) are key components of extracellular matrix (ECM) in cartilaginous tissues, specially, when linked to core proteins composing the proteoglycans [65]. Proteoglycans are reported to influence the chondrogenic activity of cells, by binding to growth factors or leading to cell-matrix interactions [66]. On the chondrogenic maturation of cells,

changes occur on the ECM, being the cartilage-specific ECM accumulated on the surrounding of differentiated chondrocytes [67].

To evaluate the chondrogenic behavior of ATDC5 in the presence of HA constructs, sulfated GAGs were quantified as a measure of ECM formation and deposition. The results obtained for sGAG (Fig. C.4, Appendix C), revealed significant differences on the materials containing nanofibres with lithium. The sGAG/DNA ratio showed that the glycosaminoglycans were upregulated in the early days of culture on the scaffolds containing fibres (Figure 9a). This behavior was more pronounced when lithium was present on the nanofibres, as the mass of sGAG was higher as Li content increased. Actually, the influence of lithium on the cartilage differentiation of human MSCs, showed by the higher production of GAG among differentiated cells was previously reported [64,68].

Over the first 7 days of culture, 5_Li and 10_Li constructs had the lowest levels of cell activity (Figure 8 and Figure C.3 -Appendix C-) but the greatest accumulation of sGAG per cell, as seen in Figure 9a. At the later time points, there is a decrease on sGAG accumulation, due to the faster increase in cell proliferation, on Li-containing scaffolds. Our hypothesis to explain this sGAGs deposition, per cell, on the early stages of culture and, on the presence of higher amounts of Li, stands on two main points: (i.) more surface contact area on HA-fibres hydrogels, allowing the accumulation of endogenous ECM proteins [69] and, (ii.) as mentioned before, the lithium inducing features on sGAGs' production.

The expression of a chondrogenic marker, the proteoglycan aggrecan, was also evaluated by Western-blotting. We can observe an increase in aggrecan expression with increasing time of culture (Figure 9b). The results suggest that the accumulation of aggrecan is higher when lithium is present in the hydrogels, however this is only observed for the longer culture periods (Figure 9b).

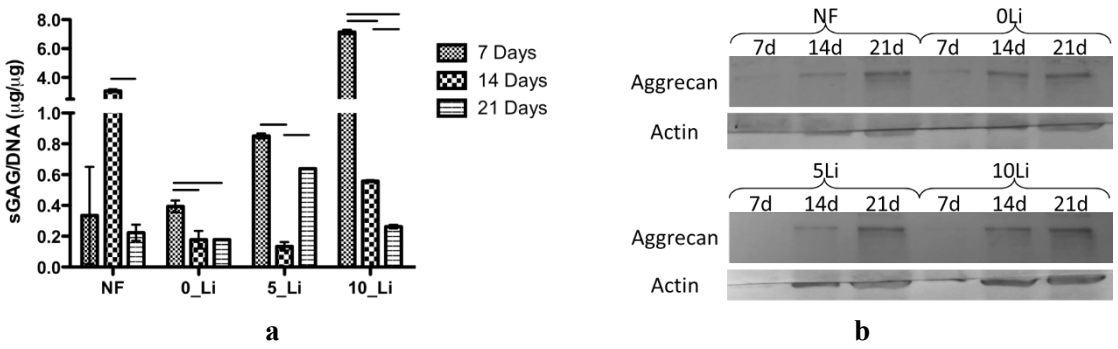

Figure 9. a) sGAG quantification of ATDC5-seeded scaffolds normalized to DNA content, cultured for 7, 14 and 21 days in basal culture (Significant statistical differences are marked for $p<0.001$). b) Effect of lithium in the expression of aggrecan by ATDC5 cells.

In conclusion, the current work demonstrates the chondrogenic potential of the lithium released from the bioactive glass micro- and nanofibres. At the same time, these fibres are able to make the HA hydrogels stiffer, thus creating a favorable microenvironment for the attachment and proliferation of chondrocytes. These synergistic effects could be modulated by modifying the amount of lithium in the fibres and/or the number of fibres in the hydrogel. Finally, the production of a nanocomposite with the fibre distribution depicted in Figure 5a (hydrogel reinforced with fibres plus fibres at the bottom and in contact with the subchondral bone) could promote the fast anchorage of the hydrogel due to the excellent bone bonding properties of the bioactive glasses. This approach could be also useful for the regeneration of subchondral defects aided by the glass dissolution products from the fibres; however, despite the good results shown in this work, potential side effects of the current approach should be discerned. For example, as reported by some works (see Refs. [70,71]), bioactive glass nano-sized materials could elicit an excessive inflammatory response during degradation. This could also occur for the current composites having bioactive glass micro- and nanofibres. However, this could be palliated by the HA hydrogel. As reported in different research works (see Refs. [72,73]), HA is recognized as having anti-inflammatory properties (dependent on the molecular weight). This or related topics should be further clarified by in-vivo tests.

4. Conclusions

In this work, we have demonstrated a new class of fibre-reinforced hydrogels, where the purpose of the fibres is two-fold, act as a mechanical reinforcement agent, and as a platform to delivery therapeutic ions to promote the healing of cartilage defects found, for example, during severe traumas or diseases. The elastic properties of hyaluronic acid hydrogels were more than triplicated using bioactive glass micro- and nanofibres produced during laser spinning. The unique characteristics of this fibre-forming technique is able to produce fibres with high-aspect ratio (with diameters in the micro- and nanometric range, and lengths in the millimetric range) and preserves the chemical composition of the bulk material. Both characteristics make possible an effective reinforcement in the studied hydrogel matrix (but also in others), and a way to obtain a sustained release of therapeutic ions. Lithium ions released in this way demonstrated to be an effective strategy to promote the chondrogenic behavior of ATDC5 cells.

Data availability

The data associated with this manuscript is available upon request to the corresponding author or the senior author.

Acknowledgements

The authors wish to thank the technical staff from CACTI (University of Vigo) for their help with sample characterization. This work was partially supported by the Government of Spain (MAT2015-71459-C2-P); the Xunta de Galicia (ED431B 2016/042, and Plan I2C Grant Program POS-A/2013/161, ED481D 2017/010 and ED481B 2016/047-0); the European Commission (H2020-TWINN-CHEM2NATURE-692333, H2020-WIDESPREAD-FoReCaST-668983 and H2020-WIDESPREAD-2016-2017-THE DISCOVERIES CTR-739572); and the Portuguese Foundation for Science and Technology (FCT) (grants SFRH/BD/112075/2015, S.A. and SFRH/BPD/85790/2012, D.S.C).

References

[1] L. Zhang, J. Hu, K.A. Athanasiou, The Role of Tissue Engineering in Articular Cartilage Repair and Regeneration, CRB. 37 (2009). https://doi.org/10.1615/CritRevBiomedEng.v37.i1-2.10.

[2] A.H. Gomoll, T. Minas, The quality of healing: Articular cartilage, Wound Repair Regen. 22 (2014) 30–38. https://doi.org/10.1111/wrr.12166.

[3] W.W. Curl, J. Krome, E.S. Gordon, J. Rushing, B.P. Smith, G.G. Poehling, Cartilage injuries: A review of 31,516 knee arthroscopies, Arthroscopy: The Journal of Arthroscopic & Related Surgery. 13 (1997) 456–460. https://doi.org/10.1016/S0749-8063(97)90124-9.

[4] T. Re'em, F. Witte, E. Willbold, E. Ruvinov, S. Cohen, Simultaneous regeneration of articular cartilage and subchondral bone induced by spatially presented TGF-beta and BMP-4 in a bilayer affinity binding system, Acta Biomaterialia. 8 (2012) 3283–3293. https://doi.org/10.1016/j.actbio.2012.05.014.

[5] M. Liu, X. Zeng, C. Ma, H. Yi, Z. Ali, X. Mou, S. Li, Y. Deng, N. He, Injectable hydrogels for cartilage and bone tissue engineering, Bone Research. 5 (2017) boneres201714. https://doi.org/10.1038/boneres.2017.14.

[6] A. Thorvaldsson, J. Silva-Correia, J.M. Oliveira, R.L. Reis, P. Gatenholm, P. Walkenström, Development of nanofiber-reinforced hydrogel scaffolds for nucleus pulposus regeneration by a combination of electrospinning and spraying technique, Journal of Applied Polymer Science. 128 (2013) 1158–1163. https://doi.org/10.1002/app.38316.

[7] K.Y. Lee, D.J. Mooney, Hydrogels for Tissue Engineering, Chem. Rev. 101 (2001) 1869–1880. https://doi.org/10.1021/cr000108x.

[8] J.L. Drury, D.J. Mooney, Hydrogels for tissue engineering: scaffold design variables and applications, Biomaterials. 24 (2003) 4337–4351. https://doi.org/10.1016/S0142-9612(03)00340-5.

[9] Q.T. Nguyen, Y. Hwang, A.C. Chen, S. Varghese, R.L. Sah, Cartilage-like mechanical properties of poly (ethylene glycol)-diacrylate hydrogels, Biomaterials. 33 (2012) 6682–6690. https://doi.org/10.1016/j.biomaterials.2012.06.005.

[10] Q. Chen, H. Chen, L. Zhu, J. Zheng, Fundamentals of double network hydrogels, J. Mater. Chem. B. 3 (2015) 3654–3676. https://doi.org/10.1039/C5TB00123D.

[11] G.D. Nicodemus, S.C. Skaalure, S.J. Bryant, Gel structure has an impact on pericellular and extracellular matrix deposition, which subsequently alters metabolic activities in chondrocyte-laden PEG hydrogels, Acta Biomaterialia. 7 (2011) 492–504. https://doi.org/10.1016/j.actbio.2010.08.021.

[12] S.R. Shin, H. Bae, J.M. Cha, J.Y. Mun, Y.-C. Chen, H. Tekin, H. Shin, S. Farshchi, M.R. Dokmeci, S. Tang, A. Khademhosseini, Carbon Nanotube Reinforced Hybrid Microgels as Scaffold Materials for Cell Encapsulation, ACS Nano. 6 (2012) 362–372. https://doi.org/10.1021/nn203711s.

[13] S. Yodmuang, S.L. McNamara, A.B. Nover, B.B. Mandal, M. Agarwal, T.-A.N. Kelly, P.G. Chao, C. Hung, D.L. Kaplan, G. Vunjak-Novakovic, Silk microfiber-reinforced silk hydrogel composites for functional cartilage tissue repair, Acta Biomaterialia. 11 (2015) 27–36. https://doi.org/10.1016/j.actbio.2014.09.032.

[14] J. Visser, F.P.W. Melchels, J.E. Jeon, E.M. van Bussel, L.S. Kimpton, H.M. Byrne, W.J.A. Dhert, P.D. Dalton, D.W. Hutmacher, J. Malda, Reinforcement of hydrogels using three-dimensionally printed microfibres, Nature Communications. 6 (2015) ncomms7933. https://doi.org/10.1038/ncomms7933.

[15] J.R. Jones, Review of bioactive glass: From Hench to hybrids, Acta Biomaterialia. 9 (2013) 4457–4486. https://doi.org/10.1016/j.actbio.2012.08.023.

[16] I.D. Xynos, A.J. Edgar, L.D.K. Buttery, L.L. Hench, J.M. Polak, Gene-expression profiling of human osteoblasts following treatment with the ionic products of Bioglass® 45S5 dissolution, J. Biomed. Mater. Res. 55 (2001) 151–157. https://doi.org/10.1002/1097-4636(200105)55:2<151::AID-JBM1001>3.0.CO;2-D.

[17] A. Hoppe, N.S. Güldal, A.R. Boccaccini, A review of the biological response to ionic dissolution products from bioactive glasses and glass-ceramics, Biomaterials. 32 (2011) 2757–2774. https://doi.org/10.1016/j.biomaterials.2011.01.004.

[18] V. Mouriño, J.P. Cattalini, A.R. Boccaccini, Metallic ions as therapeutic agents in tissue engineering scaffolds: an overview of their biological applications and strategies for new developments, Journal of The Royal Society Interface. 9 (2012) 401–419. https://doi.org/10.1098/rsif.2011.0611.

[19] S. Kargozar, F. Baino, S. Hamzehlou, R.G. Hill, M. Mozafari, Bioactive glasses entering the mainstream, Drug Discovery Today. 23 (2018) 1700–1704. https://doi.org/10.1016/j.drudis.2018.05.027.

[20] S. Nazarnezhad, F. Baino, H.-W. Kim, T.J. Webster, S. Kargozar, Electrospun Nanofibers for Improved Angiogenesis: Promises for Tissue Engineering Applications, Nanomaterials. 10 (2020) 1609. https://doi.org/10.3390/nano10081609.

[21] Y. Wu, S. Zhu, C. Wu, P. Lu, C. Hu, S. Xiong, J. Chang, B.C. Heng, Y. Xiao, H.W. Ouyang, A Bi-Lineage Conducive Scaffold for Osteochondral Defect Regeneration, Adv. Funct. Mater. 24 (2014) 4473–4483. https://doi.org/10.1002/adfm.201304304.

[22] S. Li, A.L. Maçon, M. Jacquemin, M.M. Stevens, J.R. Jones, Sol–gel derived lithium-releasing glass for cartilage regeneration, J Biomater Appl. 32 (2017) 104–113. https://doi.org/10.1177/0885328217706640.

[23] A. Zamani, G.R. Omrani, M.M. Nasab, Lithium's effect on bone mineral density, Bone. 44 (2009) 331–334. https://doi.org/10.1016/j.bone.2008.10.001.

[24] P. Clément-Lacroix, M. Ai, F. Morvan, S. Roman-Roman, B. Vayssière, C. Belleville, K. Estrera, M.L. Warman, R. Baron, G. Rawadi, Lrp5-independent activation of Wnt signaling by lithium chloride increases bone formation and bone mass in mice, PNAS. 102 (2005) 17406–17411. https://doi.org/10.1073/pnas.0505259102.

[25] H. Park, B. Choi, J. Hu, M. Lee, Injectable chitosan hyaluronic acid hydrogels for cartilage tissue engineering, Acta Biomaterialia. 9 (2013) 4779–4786. https://doi.org/10.1016/j.actbio.2012.08.033.

[26] P.A. Levett, D.W. Hutmacher, J. Malda, T.J. Klein, Hyaluronic Acid Enhances the Mechanical Properties of Tissue-Engineered Cartilage Constructs, PLOS ONE. 9 (2014) e113216. https://doi.org/10.1371/journal.pone.0113216.

[27] J.A. Burdick, G.D. Prestwich, Hyaluronic Acid Hydrogels for Biomedical Applications, Adv. Mater. 23 (2011) H41–H56. https://doi.org/10.1002/adma.201003963.

[28] I.L. Kim, R.L. Mauck, J.A. Burdick, Hydrogel design for cartilage tissue engineering: A case study with hyaluronic acid, Biomaterials. 32 (2011) 8771–8782. https://doi.org/10.1016/j.biomaterials.2011.08.073.

[29] K.L. Spiller, S.A. Maher, A.M. Lowman, Hydrogels for the Repair of Articular Cartilage Defects, Tissue Engineering Part B: Reviews. 17 (2011) 281–299. https://doi.org/10.1089/ten.teb.2011.0077.

[30] M.N. Rahaman, D.E. Day, B. Sonny Bal, Q. Fu, S.B. Jung, L.F. Bonewald, A.P. Tomsia, Bioactive glass in tissue engineering, Acta Biomaterialia. 7 (2011) 2355–2373. https://doi.org/10.1016/j.actbio.2011.03.016.

[31] B.S. Bal, M.N. Rahaman, P. Jayabalan, K. Kuroki, M.K. Cockrell, J.Q. Yao, J.L. Cook, In vivo outcomes of tissue-engineered osteochondral grafts, J. Biomed. Mater. Res. 93B (2010) 164–174. https://doi.org/10.1002/jbm.b.31571.

[32] P. Jayabalan, A.R. Tan, M.N. Rahaman, B.S. Bal, C.T. Hung, J.L. Cook, C.T. Hung, P. Jayabalan, B.S. Bal, A.R. Tan, M.N. Rahaman, Bioactive Glass 13-93 as a Subchondral Substrate for Tissue-engineered Osteochondral Constructs: A Pilot Study, Clin Orthop Relat Res. 469 (2011) 2754–2763. https://doi.org/10.1007/s11999-011-1818-x.

[33] F. Quintero, J. Pou, R. Comesaña, F. Lusquiños, A. Riveiro, A.B. Mann, R.G. Hill, Z.Y. Wu, J.R. Jones, Laser Spinning of Bioactive Glass Nanofibers, Adv. Funct. Mater. 19 (2009) 3084–3090. https://doi.org/10.1002/adfm.200801922.

[34] A. Borzacchiello, L. Russo, B.M. Malle, K. Schwach-Abdellaoui, L. Ambrosio, Hyaluronic Acid Based Hydrogels for Regenerative Medicine Applications, BioMed Research International. 2015 (2015) 1–12. https://doi.org/10.1155/2015/871218.

[35] A.A.M. Shimojo, A.M.B. Pires, R. Lichy, M.H.A. Santana, The Performance of Crosslinking with Divinyl Sulfone as Controlled by the Interplay Between the Chemical Modification and Conformation of Hyaluronic Acid, Journal of the Brazilian Chemical Society. 26 (2015) 506–512. https://doi.org/10.5935/0103-5053.20150003.

[36] S. Mondal, N. Haridas, S.S. Letha, V. Vijith, G. Rajmohan, M.J. Rosemary, Development of injectable high molecular weight hyaluronic acid hydrogels for cartilage regeneration, Journal of Macromolecular Science, Part A. 53 (2016) 507–514. https://doi.org/10.1080/10601325.2016.1189284.

[37] J.-Y. Lai, Relationship between structure and cytocompatibility of divinyl sulfone cross-linked hyaluronic acid, Carbohydrate Polymers. 101 (2014) 203–212. https://doi.org/10.1016/j.carbpol.2013.09.060.

[38] E.J. Oh, S.-W. Kang, B.-S. Kim, G. Jiang, I.H. Cho, S.K. Hahn, Control of the molecular degradation of hyaluronic acid hydrogels for tissue augmentation, J. Biomed. Mater. Res. 86A (2008) 685–693. https://doi.org/10.1002/jbm.a.31681.

[39] M. Mneimne, R.G. Hill, A.J. Bushby, D.S. Brauer, High phosphate content significantly increases apatite formation of fluoride-containing bioactive glasses, Acta Biomaterialia. 7 (2011) 1827–1834. https://doi.org/10.1016/j.actbio.2010.11.037.

[40] A.L.B. Maçon, T.B. Kim, E.M. Valliant, K. Goetschius, R.K. Brow, D.E. Day, A. Hoppe, A.R. Boccaccini, I.Y. Kim, C. Ohtsuki, T. Kokubo, A. Osaka, M. Vallet-Regí, D. Arcos, L. Fraile, A.J. Salinas, A.V. Teixeira, Y. Vueva, R.M. Almeida, M. Miola, C. Vitale-Brovarone, E. Verné, W. Höland, J.R. Jones, W. Höland, A.L.B. Maçon, E. Verné, T.B.

Kim, C. Vitale-Brovarone, E.M. Valliant, M. Miola, K. Goetschius, R.M. Almeida, R.K. Brow, Y. Vueva, D.E. Day, A.V. Teixeira, A. Hoppe, A.J. Salinas, A.R. Boccaccini, L. Fraile, I.Y. Kim, D. Arcos, C. Ohtsuki, M. Vallet-Regí, T. Kokubo, A. Osaka, A unified in vitro evaluation for apatite-forming ability of bioactive glasses and their variants, J Mater Sci: Mater Med. 26 (2015) 115. https://doi.org/10.1007/s10856-015-5403-9.

[41] H.-J. Jacobasch, G. Bauböck, J. Schurz, Problems and results of zeta-potential measurements on fibers, Colloid & Polymer Sci. 263 (1985) 3–24. https://doi.org/10.1007/BF01411243.

[42] A. Bismarck, A.R. Boccaccini, E. Egia-Ajuriagojeaskoa, D. Hülsenberg, T. Leutbecher, Surface characterization of glass fibers made from silicate waste: Zeta-potential and contact angle measurements, Journal of Materials Science. 39 (2004) 401–412. https://doi.org/10.1023/B:JMSC.0000011493.26161.a6.

[43] A.V. Delgado, F. González-Caballero, R.J. Hunter, L.K. Koopal, J. Lyklema, Measurement and interpretation of electrokinetic phenomena, Journal of Colloid and Interface Science. 309 (2007) 194–224. https://doi.org/10.1016/j.jcis.2006.12.075.

[44] S.A. Zawko, S. Suri, Q. Truong, C.E. Schmidt, Photopatterned anisotropic swelling of dual-crosslinked hyaluronic acid hydrogels, Acta Biomaterialia. 5 (2009) 14–22. https://doi.org/10.1016/j.actbio.2008.09.012.

[45] J.C. Halpin, Stiffness and Expansion Estimates for Oriented Short Fiber Composites, Journal of Composite Materials. 3 (1969) 732–734. https://doi.org/10.1177/002199836900300419.

[46] F. He, C. Ping, yuanyuan Zheng, Viscosity and Structure of Lithium Sodium Borosilicate Glasses, Physics Procedia. 48 (2013) 73–80. https://doi.org/10.1016/j.phpro.2013.07.012.

[47] R.M. Williams, H.E. Simpson, A Note on the Effect of Lithium Oxide Upon the Surface Tension of Several Silicate Melts, Journal of the American Ceramic Society. 34 (1951) 280–283. https://doi.org/10.1111/j.1151-2916.1951.tb09130.x.

[48] F. Quintero, O. Dieste, J. Pou, F. Lusquiños, A. Riveiro, On the conditions to produce micro- and nanofibres by laser spinning, J. Phys. D: Appl. Phys. 42 (2009) 065501. https://doi.org/10.1088/0022-3727/42/6/065501.

[49] M.R. DeGuire, S.D. Brown, Dependence of Young's Modulus on Volume and Structure in Alkali Silicate and Alkali Aluminosilicate Glasses, Journal of the American Ceramic Society. 67 (1984) 270–273. https://doi.org/10.1111/j.1151-2916.1984.tb18845.x.

[50] M. Tiegel, R. Hosseinabadi, S. Kuhn, A. Herrmann, C. Rüssel, Young′s modulus, Vickers hardness and indentation fracture toughness of alumino silicate glasses, Ceramics International. 41 (2015) 7267–7275. https://doi.org/10.1016/j.ceramint.2015.01.144.

[51] A. Hoppe, B. Jokic, D. Janackovic, T. Fey, P. Greil, S. Romeis, J. Schmidt, W. Peukert, J. Lao, E. Jallot, A.R. Boccaccini, Cobalt-Releasing 1393 Bioactive Glass-Derived Scaffolds for Bone Tissue Engineering Applications, ACS Appl. Mater. Interfaces. 6 (2014) 2865–2877. https://doi.org/10.1021/am405354y.

[52] T.H. Qazi, S. Hafeez, J. Schmidt, G.N. Duda, A.R. Boccaccini, E. Lippens, Comparison of the effects of 45S5 and 1393 bioactive glass microparticles on hMSC behavior, J. Biomed. Mater. Res. 105 (2017) 2772–2782. https://doi.org/10.1002/jbm.a.36131.

[53] M.F. Dilmore, D.E. Clark, L.L. Hench, Chemical Durability of Na2O-K2O-CaO-SiO2 Glasses, Journal of the American Ceramic Society. 61 (1978) 439–443. https://doi.org/10.1111/j.1151-2916.1978.tb09355.x.

[54] R. Brückner, M. Tylkowski, L. Hupa, D. S. Brauer, Controlling the ion release from mixed alkali bioactive glasses by varying modifier ionic radii and molar volume, Journal of Materials Chemistry B. 4 (2016) 3121–3134. https://doi.org/10.1039/C5TB02426A.

[55] J.O. Isard, The mixed alkali effect in glass, Journal of Non-Crystalline Solids. 1 (1969) 235–261. https://doi.org/10.1016/0022-3093(69)90003-9.

[56] J. Serra, P. González, S. Liste, C. Serra, S. Chiussi, B. León, M. Pérez-Amor, H.O. Ylänen, M. Hupa, FTIR and XPS studies of bioactive silica based glasses, Journal of Non-Crystalline Solids. 332 (2003) 20–27. https://doi.org/10.1016/j.jnoncrysol.2003.09.013.

[57] M.R. Filgueiras, G. La Torre, L.L. Hench, Solution effects on the surface reactions of a bioactive glass, J. Biomed. Mater. Res. 27 (1993) 445–453. https://doi.org/10.1002/jbm.820270405.

[58] Y. Wu, Preparation of low-molecular-weight hyaluronic acid by ozone treatment, Carbohydrate Polymers. 89 (2012) 709–712. https://doi.org/10.1016/j.carbpol.2012.03.081.

[59] S. Bhattacharyya, S. Guillot, H. Dabboue, J.-F. Tranchant, J.-P. Salvetat, Carbon nanotubes as structural nanofibers for hyaluronic acid hydrogel scaffolds, Biomacromolecules. 9 (2008) 505–509. https://doi.org/10.1021/bm7009976.

[60] M.N. Collins, C. Birkinshaw, Investigation of the swelling behavior of crosslinked hyaluronic acid films and hydrogels produced using homogeneous reactions, J. Appl. Polym. Sci. 109 (2008) 923–931. https://doi.org/10.1002/app.27631.

[61] Y. Yao, Y. Wang, ATDC5: An excellent in vitro model cell line for skeletal development, J. Cell. Biochem. 114 (2013) 1223–1229. https://doi.org/10.1002/jcb.24467.

[62] S. Ustun, A. Tombuloglu, M. Kilinc, M.O. Guler, A.B. Tekinay, Growth and Differentiation of Prechondrogenic Cells on Bioactive Self-Assembled Peptide Nanofibers, Biomacromolecules. 14 (2013) 17–26. https://doi.org/10.1021/bm301538k.

[63] D. Yunos, Z. Ahmad, V. Salih, A. Boccaccini, Stratified scaffolds for osteochondral tissue engineering applications: Electrospun PDLLA nanofibre coated Bioglass®-derived foams, J Biomater Appl. 27 (2013) 537–551. https://doi.org/10.1177/0885328211414941.

[64] M.B. Eslaminejad, N. Karimi, M. Shahhoseini, Enhancement of Glycosaminoglycan-Rich Matrix Production in Human Marrow-Derived Mesenchymal Stem Cell Chondrogenic Culture by Lithium Chloride and SB216763 Treatment, Cell J (Yakhteh). 13 (2011) 117–126.

[65] S.-H. Kim, J. Turnbull, S. Guimond, Extracellular matrix and cell signalling: the dynamic cooperation of integrin, proteoglycan and growth factor receptor, J Endocrinol. 209 (2011) 139–151. https://doi.org/10.1530/JOE-10-0377.

[66] J.K. Mouw, N.D. Case, R.E. Guldberg, A.H.K. Plaas, M.E. Levenston, Variations in matrix composition and GAG fine structure among scaffolds for cartilage tissue engineering, Osteoarthritis and Cartilage. 13 (2005) 828–836. https://doi.org/10.1016/j.joca.2005.04.020.

[67] R. Cai, T. Nakamoto, N. Kawazoe, G. Chen, Influence of stepwise chondrogenesis-mimicking 3D extracellular matrix on chondrogenic differentiation of mesenchymal stem cells, Biomaterials. 52 (2015) 199–207. https://doi.org/10.1016/j.biomaterials.2015.02.033.

[68] Z. Zhu, J. Yin, J. Guan, B. Hu, X. Niu, D. Jin, Y. Wang, C. Zhang, Lithium stimulates human bone marrow derived mesenchymal stem cell proliferation through GSK‐3β‐dependent β‐catenin/Wnt pathway activation, The FEBS Journal. 281 (2014) 5371‐5389. https://doi.org/10.1111/febs.13081.

[69] M. Ahmed, T.A. da S. Ramos, F. Damanik, B.Q. Le, P. Wieringa, M. Bennink, C. van Blitterswijk, J. de Boer, L. Moroni, A combinatorial approach towards the design of nanofibrous scaffolds for chondrogenesis, Scientific Reports. 5 (2015) srep14804. https://doi.org/10.1038/srep14804.

[70] G.E. Vargas, L.A. Haro Durand, V. Cadena, M. Romero, R.V. Mesones, M. Mačković, S. Spallek, E. Spiecker, A.R. Boccaccini, A.A. Gorustovich, Effect of nano-sized bioactive glass particles on the angiogenic properties of collagen based composites, J

Mater Sci: Mater Med. 24 (2013) 1261–1269. https://doi.org/10.1007/s10856-013-4892-7.

[71] R. Sergi, D. Bellucci, V. Cannillo, A Review of Bioactive Glass/Natural Polymer Composites: State of the Art, Materials. 13 (2020) 5560. https://doi.org/10.3390/ma13235560.

[72] C.A. Cooper, K.K. Brown, C.D. Meletis, N. Zabriskie, Inflammation and Hyaluronic Acid, Alternative and Complementary Therapies. 14 (2008) 78–84. https://doi.org/10.1089/act.2008.14201.

[73] K. Masuko, M. Murata, K. Yudoh, T. Kato, H. Nakamura, Anti-inflammatory effects of hyaluronan in arthritis therapy: Not just for viscosity, IJGM. 2 (2009) 77–81. https://doi.org/10.2147/IJGM.S5495.

Appendix A. SBF immersion tests

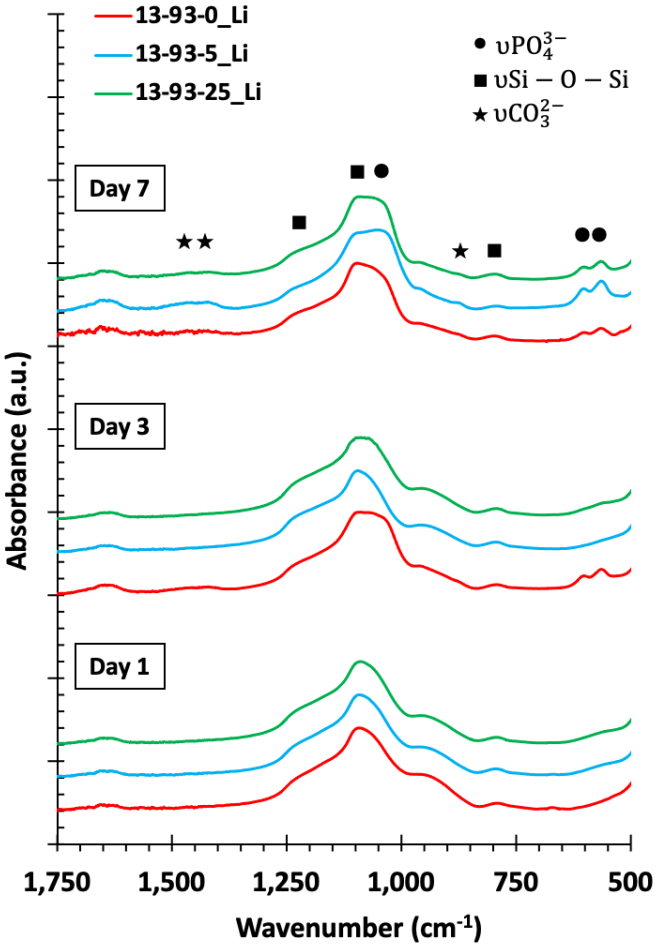

Figure A.1. FTIR spectra of bioactive glass nanofibers without lithium (13-93-0_Li) and with lithium (13-93-5_Li, 13-93-25_Li) after 1, 3 and 7 days of immersion in SBF.

The results reported here show the FTIR spectra after immersion in SBF glass fibres synthetised from a bioactive glass without lithium (13-93-0_Li) and from two bioactive glasses with different lithium content (13-93-5_Li, 13-93-25_Li). As noticed, bands associated to IR absorption of PO_4^{3-} group were observed. Bands at ~550 and ~600 cm^{-1}, characteristic of P-O bending, and at ~1025 cm^{-1}, characteristic of P-O stretching were detected. The bands detected at ~1450 cm^{-1}, ~1410 $cm^{-1}$and ~865 cm^{-1} were associated to the CO_3^{2-}group of B-type carbonated apatite. This confirms the formation of hydroxy-carbonate apatite on the surface of all the glass fibres after immersion in SBF.

As observed in these spectra, apatite formation is delayed up to the day 7 for the glass fibres containing lithium; however, the formation of apatite is detected after 3 days of immersion in SBF for glass fibres without any lithium content. This could be attributable to the more compact network result of the introduction of an alkali ion of small ionic radius such as Li+.

Appendix B. Halpin-Tsai equations

The value of the elastic moduli G' obtained through rheology was compared with the theoretical predictions given by the Halpin-Tsai equations [1]. These empirical relationships enable the calculation of the elastic modulus of a composite material in terms of the elastic modulus of the matrix and reinforcing phases together with their proportions and geometry. In the present case, the elastic modulus of the HA hydrogels reinforced with the fibres E_c is calculated in terms of the elastic moduli of the HA hydrogels E_{hyd} and the glass fibres E_{fib} through the following relationships:

$$E_c = E_{hyd}\left(\frac{1+\xi\eta f}{1-\eta f}\right) \qquad \text{with} \qquad \eta = \frac{\left(\frac{E_{fib}}{E_{hyd}}\right)-1}{\left(\frac{E_{fib}}{E_{hyd}}\right)+\xi} \qquad \text{(Eq. B.1)}$$

The calculation of the elastic modulus thorough these expressions depends on the volume fraction of fibres $f = {V_{fib}}/{\left(V_{fib} + V_{hyd}\right)}$ (with V_{fib} and V_{hyd} the volume occupied by the glass fibres and the HA hydrogel respectively), and on the parameter ζ which takes into account the geometry and orientation of the filler material into the composite. The parameter ζ proposed by Halpin for the determination of the elastic modulus of a composite (for composites with a volume fraction of fibres f<0.4) in the same direction of the fibres $E_{c,11}$, and in the direction perpendicular to the fibres $E_{c,22}$ is, respectively:

$$\xi_{11} = 2\left(\frac{L}{D}\right) \qquad \text{(Eq. B.2)}$$

$$\xi_{22} = 2 \qquad \text{(Eq. B.3)}$$

with L, and D the length and diameter of the fibres respectively. Therefore $\frac{L}{D}$ represents the aspect ratio of the fibres. The elastic modulus of the composite in the same direction of the fibres $E_{c,11}$, and in the direction perpendicular to the fibres $E_{c,22}$ is obtained from the equation (Eq. B.1) using alternatively the expressions (Eq. B.2) or (Eq. B.3).

In the present case, the fibres are randomly oriented into the HA hydrogels, which allows for the estimation of the overall elastic modulus through the following expression proposed by Kardos [2]:

$$E_c = \frac{3}{8}E_{c,11} + \frac{5}{8}E_{\ c,22} \qquad \text{(Eq. B.4)}$$

The following values were used for the calculations: E_{hyd}=1851 Pa (see Table 3, HA hydrogel), E_{fib}=3.85E+9 Pa (Figure 2b, composition:13-93-0_Li), L=1000 μm (mean length of fibres in the mm range), D=1 μm (mean diameter of fibres in the μm range), V_{hyd}=0.12 cm^3 (120 μL of HA solution used in each cylindrical hydrogel), V_{fib}=0.00008, 0.0002, and 0.0004 cm^3 for the gels with 0.2, 0.5 and 1.0 mg of fibres, i.e. 4/100, 10/100 and 20/100 fibers to HA mass ratio (volume estimated using a glass density of 2.5 g/cm^3)

References for Appendix B

[1] J.C. Halpin, Stiffness and Expansion Estimates for Oriented Short Fiber Composites, Journal of Composite Materials. 3 (1969) 732–734. https://doi.org/10.1177/002199836900300419.

[2] J.L. Kardos, Critical issues in achieving desirable mechanical properties for short fiber composites, Pure and Applied Chemistry. 57 (2009) 1651–1657. https://doi.org/10.1351/pac198557111651.

Appendix C. Supplementary data

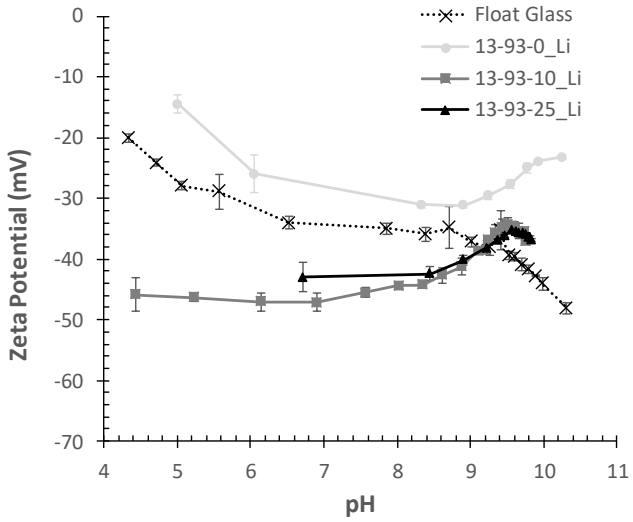

Figure C.1. Variation of the zeta potential with pH for the glass fibres (zeta potential for float glass fibres produced by laser spinning technique under identical processing conditions is included for comparison purposes).

The results reported here show that the zeta potential of the glass fibres was always negative at acidic, neutral and basic pH values. The negative values in this parameter can be related to the chemical composition of the glass, fibre size and the surrounded environment. On the other hand, the zeta potential increased with the lithium content.

The zeta potential for the 13-93 glass fibres (with or without lithium) did not follow the typical decrease with pH, as observed for example in micro- and nanofibres made from float glass (included in Figure S1 for comparison purposes), but increased. The zeta potential, e.g. for the 13-93-0_Li and 13-93_25_Li fibres, increased from -28 and -42 mV (at pH=7) up to -24 and -36 mV (at pH=10), respectively. This is explained due to the lower corrosion resistance of the 13-93 glass system as compared, for example, with float glass. The dissolution of network modifier cations (accompanied by surface rearrangements), and their impact on the electrochemical double layer cause an increase in the zeta potential [1]. Lu *et al.* hypothesized

that the negative glass surface could trap ions (e.g. Na^{+}, Ca^{2+}) leaching from the bulk glass or from the solution [2]. This would be responsible for the formation of a Ca-P layer on the glass surface. These authors corroborated this increase during the first 24 h of immersion of 45S5 bioactive glass into a Tris/HCl electrolyte solution. This increase in the zeta-potential coincided with the formation of an amorphous Ca-P layer on the glass.

A negative zeta potential has been showed to be biologically relevant *in vivo* and *in vitro* according to different studies [3, 4]. Biomaterials showing a negative zeta potential (i.e. an electronegative surface charge) showed better attachment and proliferation of osteoblasts. Smeets *et al.* have proposed that these negative charges promote a rapid attachment of proteins with chemotactic and adhesive properties on the surface of the biomaterial; therefore, the surface is accessible for a fast attachment of osteoblast [3].

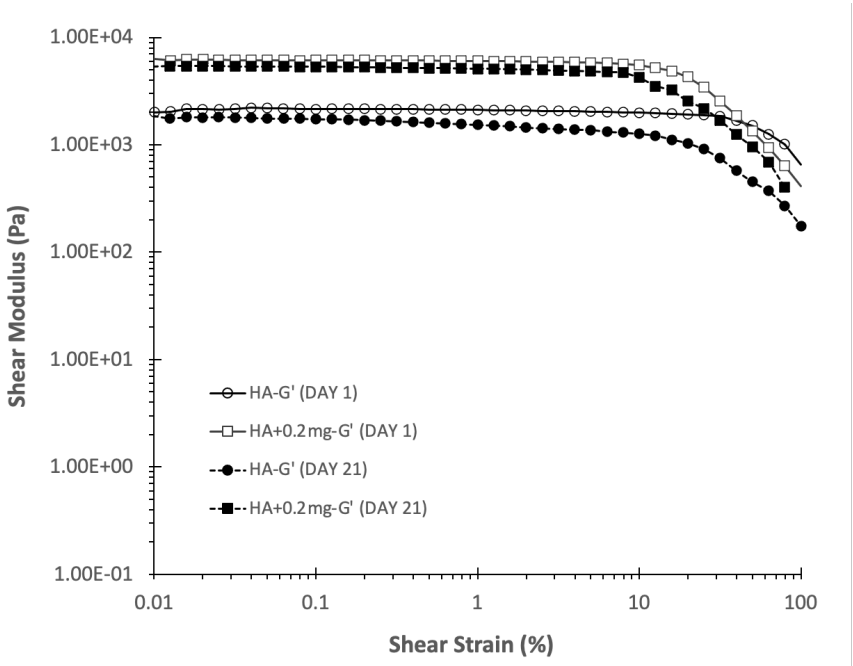

Figure C.2. Strain sweep (at 1 Hz) for HA hydrogels crosslinked with DVS with at without fibers (composition: 13-93-0_Li, 0.2 mg of fibers, 4/100 ratio) at different times (1 and 21 days).

The measurement of the elastic modulus (G') for the hydrogels loaded with and without fibres over the time (see Fig. C.2) shows that the elastic modulus is slightly decreased over time; however, this decrease is not excessive after 21 days of crosslinking. Furthermore, the mechanical properties of hydrogels loaded with fibres are higher than those without fibres over the studied time.

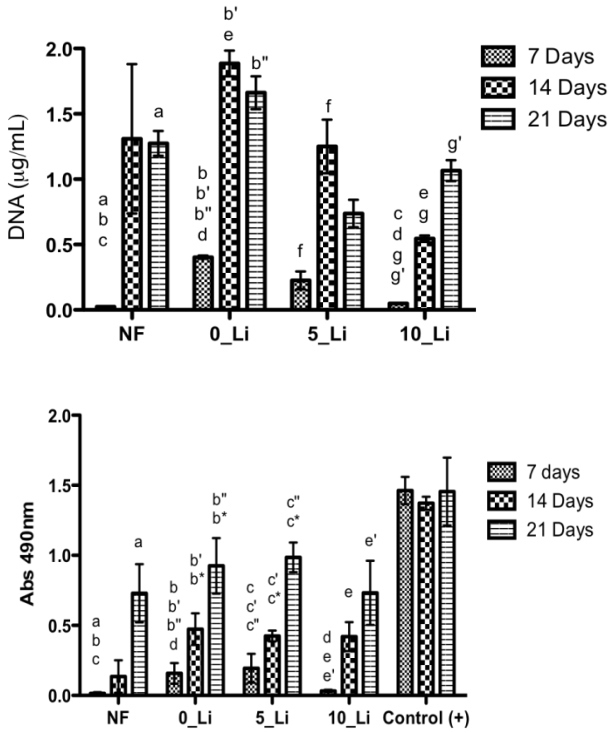

Figure C.3. ATDC5 proliferation (DNA quantification) and viability (MTS quantification) at 7, 14, and 21 days after seeding. Significant differences were represented by letters for $p < 0.001$, as determined by the statistical analysis.

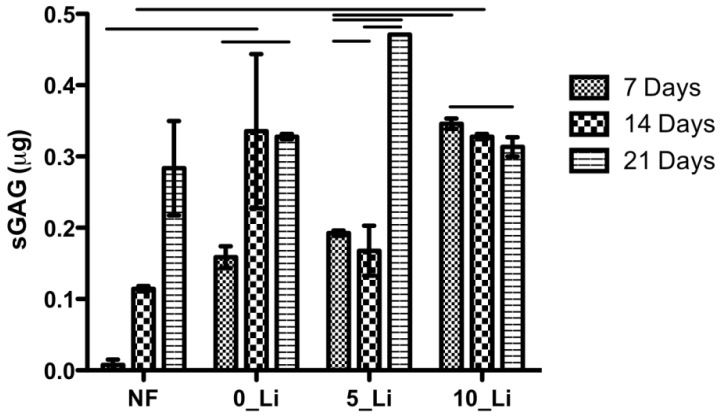

Figure C.4. Total sulphated GAGs quantification of ATDC5-seeded scaffolds cultured for 7, 14 and 21 days in basal culture. Significant statistical differences are marked for $p<0.001$.

References for Appendix C

[1] A. Bismarck, A.R. Boccaccini, E. Egia-Ajuriagojeaskoa, D. Hülsenberg, T. Leutbecher, Surface characterization of glass fibers made from silicate waste: Zeta-potential and contact angle measurements, Journal of Materials Science. 39 (2004) 401–412. https://doi.org/10.1023/B:JMSC.0000011493.26161.a6.

[2] H.H. Lu, S.R. Pollack, P. Ducheyne, Temporal zeta potential variations of 45S5 bioactive glass immersed in an electrolyte solution, J. Biomed. Mater. Res. 51 (2000) 80–87. https://doi.org/10.1002/(SICI)1097-4636(200007)51:1<80::AID-JBM11>3.0.CO;2-6.

[3] R. Smeets, A. Kolk, M. Gerressen, O. Driemel, O. Maciejewski, B. Hermanns-Sachweh, D. Riediger, J.M. Stein, A new biphasic osteoinductive calcium composite material with a negative Zeta potential for bone augmentation, Head & Face Medicine. 5 (2009) 13. https://doi.org/10.1186/1746-160X-5-13.

[4] A. Doostmohammadi, A. Monshi, R. Salehi, M.H. Fathi, Z. Golniya, Alma.U. Daniels, Bioactive glass nanoparticles with negative zeta potential, Ceramics International. 37 (2011) 2311–2316. https://doi.org/10.1016/j.ceramint.2011.03.026.